USING SPACE BORNE MICROWAVE SENSORS TO TRACK LARGE ANTARCTIC ICEBERGS

by

Jarom J. Ballantyne

A thesis submitted to the faculty of

Brigham Young University

in partial fulfillment of the requirements for the degree of

Master of Science

Department of Electrical and Computer Engineering

Brigham Young University

April 2002

BRIGHAM YOUNG UNIVERSITY

GRADUATE COMMITTEE APPROVAL

of a thesis submitted by

Jarom J. Ballantyne

This thesis has been read by each member of the following graduate committee and by majority vote has been found to be satisfactory.

Date	Dr. David G. Long, Chair
Date	Dr. Mark L. Manwaring
Date	Dr. Karl F. Warnick

BRIGHAM YOUNG UNIVERSITY

As chair of the candidate's graduate committee, I have read the thesis of Jarom J. Ballantyne in its final form and have found that (1) its format, citations, and bibliographical style are consistent and acceptable and fulfill university and department style requirements; (2) its illustrative materials including figures, tables, and charts are in place; and (3) the final manuscript is satisfactory to the graduate committee and is ready for submission to the university library.

Date

Dr. David G. Long
Chair, Graduate Committee

Accepted for the Department

Dr. A. Lee Swindlehurst
Graduate Coordinator

Accepted for the College

Dr. Douglas M. Chabries
Dean, College of Engineering and Technology

ABSTRACT

USING SPACE BORNE MICROWAVE SENSORS TO TRACK LARGE ANTARCTIC ICEBERGS

Jarom J. Ballantyne

Department of Electrical and Computer Engineering

Master of Science

Studying Antarctic icebergs can provide insight into climatic changes of the Earth's frozen continent. Antarctic icebergs are regularly formed by the separation of massive sections of ice from ice shelves and glaciers.

The National Ice Center (NIC) is playing a major role in sea ice analysis and forecasts. As a part of its mission the NIC is using a variety of satellite sensors to track many large Antarctic icebergs. The NIC reports iceberg positions every 15-20 days. However, there are limitations in the NIC's iceberg tracking techniques. The areas covered by the images used by the NIC are limited to specific areas of the Antarctic continent, due in part to the resources required to produce and process these high resolution images.

Based on the NIC data base, the number of large Antarctic icebergs seems to be increasing in recent years. This leads to a concern of a possible climatic trend. However, our analysis of historic scatterometer and radiometer data suggests this increase is largely due to improved resources and technological advancements for

iceberg tracking. Additionally several major iceberg calving events have taken place in recent years. These calving events may represent natural variability.

To evaluate the NIC's tracking and to monitor recent iceberg activity, we used current and historic scatterometer and radiometer data to track Antarctic icebergs spanning nearly 25 years. Five data sets from various instruments were used in the study. Icebergs were tracked independently with each data set for time periods between 1976 to 2001. Each image provides coverage of the entire Antarctic continent allowing frequent positions to be reported for each iceberg. The results show that the number of large icebergs over the last 20-25 years has remained fairly constant with the exception of an increase in icebergs from 1994 to 2001 due to several major calving events on the Filchner, Ronne, and Ross ice shelves. Our increased ability to observe and track the formation of large Antarctic icebergs using remote satellite sensors has contributed significantly to our awareness of these icebergs.

ACKNOWLEDGMENTS

I would like to first acknowledge Professor David Long, who introduced me to the field of remote sensing. He had the vision to take me on as a research assistant when I was an inexperienced undergraduate. He has taught me many valuable principles of research that will serve as the foundation for my career.

I greatly value the associations that I obtained in the MERS lab. I grew intellectually by interacting with its talented students, and I feel that I have gained many life-long friends. Particular thanks to David Draper. His advice and listening ear were invaluable.

Contents

List of Tables

List of Figures

Chapter 1

Introduction

Many methods have been used to track and study Antarctic icebergs. The research described in this thesis provides a new method for understanding and applying remotely sensed data to iceberg studies. The resulting contributions are an additional tool in understanding the behavior and improving the tracking method of Antarctic icebergs.

Some of the most valuable tools in studying polar sea ice are spaceborne microwave radiometers and scatterometers. The Nimbus-5 Electronically Scanning Microwave Radiometer (ESMR) was among the earliest microwave radiometers. It monitored the passive microwave emissions from sea ice and other surfaces. The Nimbus-7 Scanning Multichannel Microwave Radiometer (SMMR) was later launched and added to the passive microwave observations of the earth. The series of Special Sensor Microwave Imagers (SSM/I) aboard Defense Meteorological Satellite Program (DMSP) platforms was later included.

Microwave radiometers, such as the Special Sensor Microwave/Imager (SSM/I), have multiple applications in remote sensing over the ocean. SSM/I data has been used for land and ice studies, including snow-cover classification, measurements of soil and plant moisture content, atmospheric moisture over land, land surface temperature, and polar ice mapping. The relatively low resolution of SSM/I images is improved with the help of resolution-enhancement algorithms.

Scatterometers also play an important part in studying the polar regions. Scatterometry was first discovered in radar in WWII. Some of the earliest radar measurements over the oceans were cluttered by apparent sea noise. It was later

learned that the clutter was a response to the wind generated waves over the oceans. In 1960's the mid incidence angle radar response was related to wind speed and direction. From radar scattering measurements the wind could be determined.

The first scatterometer flew in 1973 and 1974 as part of the Skylab missions. This was the first demonstration of spaceborne scatterometer wind retrieval. The Seasat-A Satellite Scatterometer (SASS) was the first spaceborne wind scatterometer and was operational from June 1978 to October of the same year. Accurate wind measurements were made using SASS which prompted future missions. Later the European Space Agency's Remote Sensing Satellite-1 (ERS-1) carried a single-swath C-band scatterometer. The NASA Scatterometer (NSCAT) was launched aboard Japan's ADEOS-Midori satellite in August 1996. NSCAT was a dual-swath, Ku-band scatterometer. NSCAT operated from September 1996 until June 1997 when the mission was prematurely terminated due to satellite power loss. During its operation NSCAT performed flawlessly and returned unprecedented coverage, resolution, and accuracy in determining the ocean wind speed and direction. The QuikSCAT mission, a fast follow-on to NSCAT, was launched in 1999. The SeaWinds scatterometer is a microwave radar specialized to measure near-surface wind speeds over the Earth's oceans regardless of weather and cloud conditions. As with SSM/I data, the relatively low resolution of the scatterometer data can be improved with resolution enhancement also. Enhanced resolution images are produced with the help of Brigham Young University's (BYU) Scatterometer Image Reconstruction (SIR) algorithm.

The lower frequencies inherent to the microwave portion of the spectrum are less sensitive to atmospheric distortions such as cloud cover and precipitation than optical or infrared instruments. Therefore microwave instruments have an advantage over optical and infrared sensors. This is a great benefit to regions such as the Arctic and Antarctic that are frequently covered with clouds. Microwave sensors do not require solar illumination to collect measurements of the Earth's surface. This is another critical feature for polar remote sensing instruments since the polar regions experience months of complete darkness each year.

1.1 The Importance of Studying and Tracking Antarctic Icebergs

The earth's cryosphere consists of the polar regions and ice-covered areas of the globe. Scientists are interested in monitoring the properties of icebergs in these areas due to their direct influence on short-term weather patterns, long-term climate change, and shipping in the southern oceans. The properties of sea and glacial ice are critical in this system. Some scientists believe that glacial ice is an indicator of long term global climate change. Therefore, if the earth experiences a long term cooling or warming trend, one of the first symptoms will be observed in the number of Antarctic icebergs. For example, above average temperatures during the Antarctic summer months create water-filled crevasses that cause ice fractures in ice shelves and glaciers. Icebergs are then formed when stress from winds and tides cause sections of ice to break from the ice shelves or glaciers. Several Antarctic ice shelves are experiencing major retreats as a result of major caving events. Also, glacial ice from ice shelves provide a source of fresh water which directly influences the population distributions and sizes of polar biota. Finally, knowing the positions of Antarctic icebergs can help mariners in the southern ocean avoid hazards. For example during the summer of 1999 a large iceberg entered shipping lanes between the Antarctic peninsula and South America. The iceberg, named B10A, measured 24 by 48 statute miles and posed a threat for mariners operating in the southern oceans. Hundreds of smaller icebergs broke off when it moved into warmer water prompting a cautionary zone 165 miles in radius around the center point of B10A.

The harsh environment and vast size of the polar regions creates difficulties with the collection of in situ position measurements for icebergs. However, satellite microwave remote sensing provides an ideal method for locating the position of icebergs in these regions. Complete coverage of the polar regions can typically be achieved in just a few days with these instruments. Despite the relatively low resolution of many of the sensors, all of them provide information for tracking Antarctic icebergs that is otherwise unavailable.

1.2 Description of the Problem

Advances of modern technology allow researchers to monitor the polar regions of the earth without having to endure the trials of Arctic and Antarctic weather. While in situ measurements are still important, satellite remote sensing gives scientists the ability to study the polar regions in ways otherwise not possible.

An accurate knowledge of the locations and numbers of Antarctic icebergs is critical to understanding the polar regions and how they effect the rest of the planet. Providing accurate and timely measurements of iceberg positions is crucial to providing warnings to mariners and is a major part of this research.

Numerous methods have been used to track icebergs. Location markers can be used to locate icebergs but they are not practical since their deployment requires actual visits to each iceberg. Since icebergs are very dynamic these markers or beacons can either be washed away or dislodged from the iceberg. Aerial reconnaissance is another method used to track icebergs. However, the iceberg's position can significantly change between reported positions.

The National Ice Center (NIC) plays a major role in tracking the location of Antarctic icebergs. The NIC uses a variety of satellite sensors to track many large icebergs. However, there are limitations to the NIC's iceberg tracking techniques. Times between reported positions can vary from 15-20 days. Also, the areas covered by the images used by the NIC are limited to specific areas of the Antarctic continent, due in part to the resources required to produce and process these high resolution images. A major focus of this thesis is to develop a more efficient iceberg tracking and monitoring technique.

Based on the NIC data base, the number of large Antarctic icebergs seems to be increasing in recent years. This leads to a concern of a possible climatic trend, though the increase may also represent reasonable variability. This increase may also be due to improved resources and technological advancements for iceberg tracking.

In order to evaluate these results and monitor recent iceberg activity a series of passive and active microwave sensors are used. Microwave sensors are also less sensitive to atmospheric distortions than optical satellite sensors. For many current

sensors these benefits come at the expense of spatial resolution. Image reconstruction techniques are used to enhance the spatial resolution of the low resolution sensor data. The reconstruction techniques used produce a standard set of different images that can be use to study the icebergs. Determining which type of image is optimal for tracking and monitoring icebergs is a major focus of this thesis.

1.3 Research Contributions

Several contributions are made by this research in utilizing active and passive microwave remote sensors for monitoring and tracking large Antarctic icebergs. Radiometer and scatterometer data sets are evaluated for their usefulness in iceberg tracking and are compared with other methods. A semi-automated tracking technique is developed to use with the scatterometer and radiometer data sets. The contributions are considered below.

The first contribution comes from evaluating the use of enhanced resolution passive radiometer images for tracking and studying icebergs. Seven different images from SSM/I's seven channels are evaluated for tracking Antarctic icebergs. The higher frequency channels provide a better resolution but are much noisier than lower frequency channels. This study shows that even though the higher frequency channels have a better resolution, the lower frequency channels provide the best results for tracking icebergs. Variations in iceberg brightness temperature (T_b) values are also studied to determine the T_b relationship between icebergs, sea ice and open ocean. Understanding this relationship helps to determine the location of the icebergs using SSM/I data.

Another contribution of this thesis is the utilization of scatterometer data from the QuikSCAT, SASS, NSCAT, and ERS1/2 satellites to track and monitor Antarctic icebergs. Using enhanced resolution scatterometer images, sea ice, ice shelves, and land features can be clearly seen as σ^0 values vary across the Earth's surface. Antarctic icebergs can be identified as objects of high backscatter against the lower backscatter of sea ice or ocean. In order to determine the feasibility and reliability of using QSCAT images for tracking Antarctic icebergs a set of 14 different icebergs were

tracked for approximately one year (2000) using eight different QSCAT image types. The icebergs were selected from different parts of the Antarctic continent to give a broad perspective on the ability to track icebergs in each area. Tradeoffs for using each image type are considered. Knowing the relationship between winds, icebergs, and ice shelves may play an important role in understanding a larger system of global ocean currents which transport water, heat, and salt around the world.

The final contribution is a multidecadal study of the number of Antarctic icebergs using scatterometer data. To evaluate the NIC's tracking and to monitor recent iceberg activity, current and historic scatterometer and radiometer data were used to track Antarctic icebergs spanning nearly 25 years. Five data sets from various instruments were used in the study. Icebergs were tracked independently with each data set for time periods between 1978 to 2001. Each image provides coverage of the entire Antarctic continent allowing frequent positions to be reported for each iceberg. The results show that the number of icebergs over the last 20-25 years has remained fairly constant with the exception of an substantial increase in icebergs from 1999 to 2001 due to several major calving events on the Filchner, Ronne, and Ross ice shelves. Our increased ability to observe and track the formation of large Antarctic icebergs using remote satellite sensors has contributed significantly to our awareness in the number of icebergs and is a key reason for the increase in the NIC database. This study shows the advantages and limitations of tracking icebergs using scatterometer data.

This thesis research provides important contributions to studying icebergs using remote sensing techniques. Questions about the feasibility of tracking icebergs using scatterometer and radiometer data are addressed and compared with other methods used. The results of these studies reveals many interesting features about the behavior of icebergs in the southern hemisphere.

1.4 Thesis Outline

The research documented in this thesis covers various Antarctic iceberg studies. Each study provides important results on the behavior of icebergs and the use of

remote satellite data in tracking many Antarctic icebergs. A brief overview of each chapter is given in the following paragraphs.

Chapter 2 presents general background information for the studies to be considered. A brief history of polar microwave remote sensing is given. Specifications of the various instruments used to collect microwave data from the Earth's surface are reported. The scatterometer image reconstruction algorithm used to generate enhanced resolution imagery for each study is described.

In Chapter 3 SSM/I images are evaluated for their usefulness in tracking Antarctic icebergs. In this report, results are presented from the observation of several icebergs during 1999-2000 using the Defense Meteorological Satellite Program's (DMSP) radiometer SSM/I. Multichannel analysis shows a tradeoff between high resolution and low resolution images.

In Chapter 4 QSCAT images are evaluated for their usefulness in tracking Antarctic icebergs. Results provide information on the temporal and spatial behavior of several icebergs during 2000 using NASA's scatterometer SeaWinds on the spaceborne satellite QuikSCAT (QSCAT). Multi-image analysis shows the similarities and differences between the types of images produced. The QSCAT images reveal the effect of katabatic winds on icebergs and ice shelves.

Finally, Chapter 5 contains a multidecadal study of the number of Antarctic icebergs using scatterometer data. Based on the NIC iceberg database the number of large Antarctic icebergs seems to be increasing in recent years. To evaluate in NIC's tracking and monitor recent iceberg activity, current and historic scatterometer data is used to track Antarctic icebergs spanning nearly 25 years. Icebergs were tracked independently with each data set for the time periods between 1976 to 2001. This study shows that the increased ability to observe and track the formation of large icebergs using remote satellite sensors has contributed significantly to our awareness of changes in the number of large icebergs in the Antarctic region.

Chapter 2

Background

Remote sensing has become a valuable tool in studying Antarctic icebergs. Many past and current instruments have demonstrated the ability to tracking these icebergs. This chapter consists of a brief background and history of low-resolution spaceborne microwave remote sensing instruments. Due to the low spatial resolution of microwave scatterometer and radiometer data, resolution enhancement algorithms are used. This image reconstruction method is also introduced.

2.1 Active Microwave Remote Sensing

Spaceborne scatterometers have historically been used to determine ocean surface wind vectors. Small ripples called capillary waves are generated by ocean surface winds as energy is transferred from wind to water. These capillary waves have a wavelength of a few centimeters. Often these capillary waves are super imposed on other types of waves. Capillary waves are of particular interest because they are related to the winds that created them.

The main function of the scatterometer is to measure the strength of the radar backscatter. After the scatterometer transmits a microwave pulse to the ocean surface, some of the energy is scattered and some is reflected back to the instrument. Typically the rougher the surfaces due to winds the more energy is scattered back to the scatterometer. The normalized radar backscatter, σ^o, is a measurement of the returned energy. Estimates of the wind vectors are obtained as measurements are taken from several azimuth angles.

The rapid repeat coverage and the low spatial resolution of these sensors provide an ideal tool for studying such a large scale phenomena. Many non-ocean surface studies have also been done using spaceborne microwave scatterometers [3, 4].

The transmitted and received power are related through the radar equation [2],

$$P_r = (P_t G^2 \lambda^2 A \sigma^0)/((4\pi)^3 R^4 L), \tag{2.1}$$

where P_t is the power transmitted, P_r is the received backscattered power, L represents system losses, G is the antenna and receiver gain, λ is the wavelength of the transmitted pulse, A is the effective illuminated surface area, R is the distance from the scatterometer to the target, and σ_0 is the normalized radar cross section of the surface. The first seven of these parameters are related to the sensor. The normalized radar cross section is a function of both system and surface parameters.

Scatterometer backscatter is mainly a function of surface geometry or roughness and dielectric properties. For icebergs and sea ice there are several fundamental factors that affect the scattering properties [3],

- Surface roughness,
- Multilayer structure (including thickness) and the effective permittivities of those layers,
- Water content,
- Volume scatter shape, distribution, size and permittivity.

Within an incidence angle range of $[20^0, 55^0]$, σ_0 is approximately a linear function of θ,

$$\sigma^0(\theta) = A + B(\theta - 40^0) \tag{2.2}$$

where A is the normalized radar backscatter at 40^0 incidence angle while B describes the dependence of σ^0 on the incidence angle. Valuable information about surface geophysical parameters are contained in A and B.

Several microwave scatterometers have demonstrated their usefulness in monitoring sea and glacial ice [5, 6, 7, 8, 9, 10, 11, 12, 13, 14, 15, 16, 17, 18]. The following sections describe the scatterometers that were used in this thesis.

2.1.1 The Seasat-A Scatterometer (SASS)

The Seasat-A scatterometer (SASS) was the first spaceborne scatterometer to monitor the Antarctic regions of the earth. This dual-polarization Ku-band (14.6 GHz) scatterometer had a fan beam configuration that collected σ^0 measurements over wide areas from two side-looking swaths [19]. Figure 2.1 shows the SASS multiple fan beam geometry. Doppler filtering is used to enhance the resolution resulting in numerous 25-50 km resolution measurement cells for each beam.

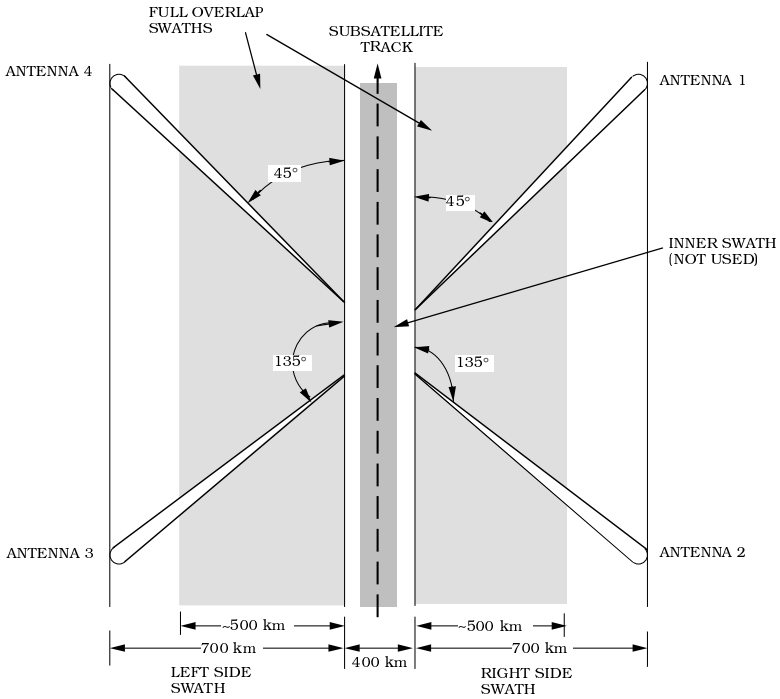

Figure 2.1: *SASS multiple fan beam geometry.*

The SASS instrument was launched in 1978 and was originally designed to estimate wind speeds and directions over the ocean surface using measured σ^0 values. Yet, it was soon found that SASS displayed important variations over land and sea ice that proved useful for monitoring surface features. A study by Long and Drinkwater monitored glacial ice in Greenland using enhanced resolution SASS σ^0 observations [5]. Being the first earth remote sensing scatterometer, SASS has been used in change studies in the Antarctic and Arctic. SASS, ERS-1/2, and NSCAT were used to determine the long term changes in polar ice sheets [6]. Drinkwater and Carsey monitored the summer to fall transitions in sea ice σ^0 [20] showing the effects of freezing on backscattered values.

Due to a system failure the SASS mission was terminated early. Only about 100 days of data were collected during this mission. However, SASS proved that scatterometers can be very valuable in ocean, land, and ice studies.

2.1.2 The European Remote Sensing Satellites (ERS-1 and ERS-2)

After the loss of SASS there was not an active spaceborne scatterometer for over two decades. In 1991 the European Space Agency launched the first European Remote Sensing Satellite (ERS-1). Including other instruments, the ERS-1 carries a C-band (5.3 GHz) scatterometer called the active microwave instrument (AMI) [7]. At several azimuth and incidence angles the AMI measures vv-polarization (vv-pol) σ^0. As shown in Figure 2.2 this instrument has a single side looking swath with tree antennas at various azimuth and incidence angles. Using range gating the fan beam resolutions are broken into measurement cells with an effective cell spatial resolution approximately 50 km. In 1996 an identical AMI scatterometer was launched aboard a similar platform, ERS-2.

The ERS scatterometer data has proven useful for a variety of wind, land, and ice studies. Gohin and Cavanie used ERS-1 data to determine sea ice types [8]. In [9], ERS-1 data values of Antarctic sea ice were used with passive signatures to find similarities and differences in sensor sensitivities to sea ice features. Enhanced resolution imaging of Antarctic sea ice packs with the ERS-1 scatterometer is examined in [10].

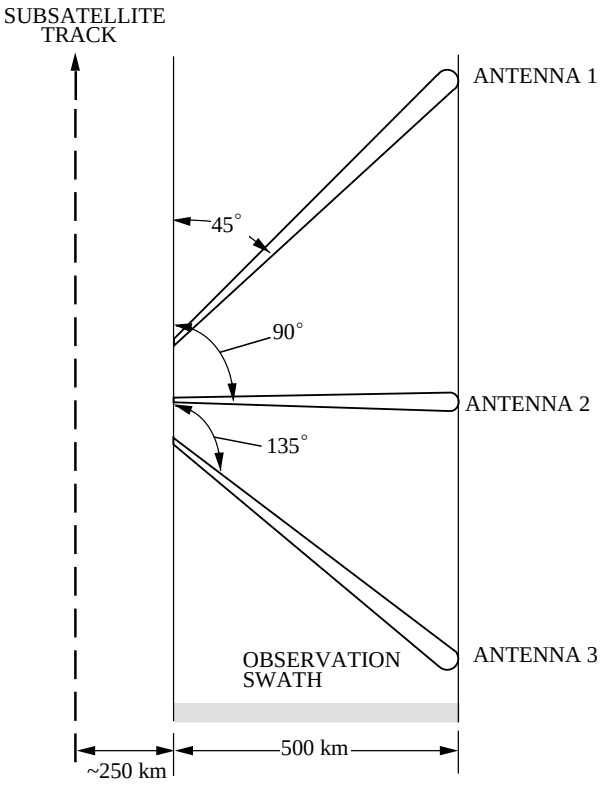

Figure 2.2: *ERS AMI scatterometer multiple fan beam geometry.*

Early and Long [11] studied Antarctic ice to evaluate azimuthal modulation levels at C-band. This study showed an azimuthal dependence of σ^0 in glacial ice regions and negligible modulation over sea ice. Finally, Ulander et al. [12] looked at the effects of frost flowers on young ice and how these features cause SAR σ^0 signatures that are similar to older deformed ice types.

2.1.3 The NASA Scatterometer (NSCAT)

NSCAT was launched on August 16, 1996, aboard the Advanced Earth Observing Satellite (ADEOS). NSCAT uses an array of six 3-meter-long antennas that radiate microwave pulses at a frequency of 14 GHz (Ku-band) across the Earth's surface as shown in Figure 2.3. NSCAT obtains backscatter almost continuously recording 190,000 wind measurements per day.

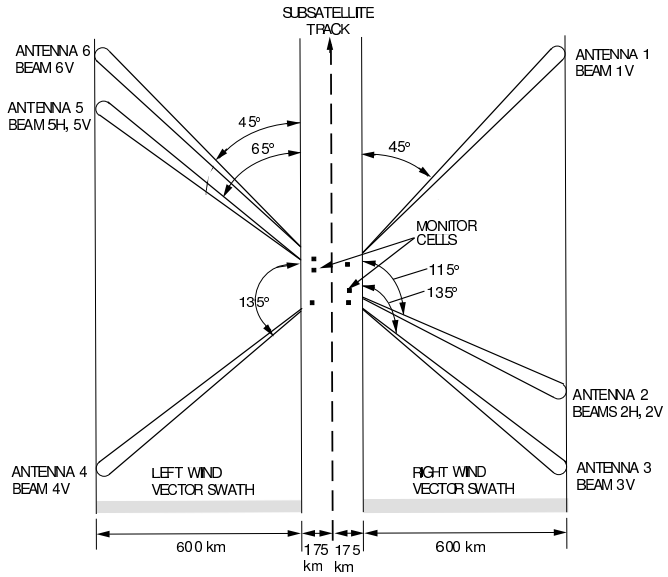

Figure 2.3: *NSCAT multiple fan beam geometry.*

The NSCAT scatterometer is an advanced version of the previous scatterometer Seasat SASS. Both scatterometers are Ku-band Doppler radars and both use a stick-type antenna design. The six stick-type antennas on NSCAT are oriented to give three different azimuth looks on each side of the satellite rather than two azimuth looks with SASS's four beam configuration shown in Figure 2.1. NSCAT provides dual polarized beams for two of the antennas giving the instrument 6 vv-pol and 2 hh-pol beams. This gives it a different azimuth look, and improves its wind retrieval capabilities. NSCAT has a higher resolution while measuring backscatter at 25 km and wind vectors at 50 km (and 25 km) resolution. The SASS resolutions are 50 km to 100 km for backscatter and wind measurements. The cell power binning for NSCAT is a function of the satellites orbital position. The on-board processor calculates the frequency shift for each dell as a function of time from the equator crossing. Figure 2.4 shows a sample NSCAT cell along with the beam width and Doppler filtering responses.

NSCAT data sets have been very useful in many land and ice studies. For example Long and Drinkwater [13] monitored sea ice edges and examined the correlation of NSCAT σ^0 with local temperatures and precipitation events. Yueh and Kwok

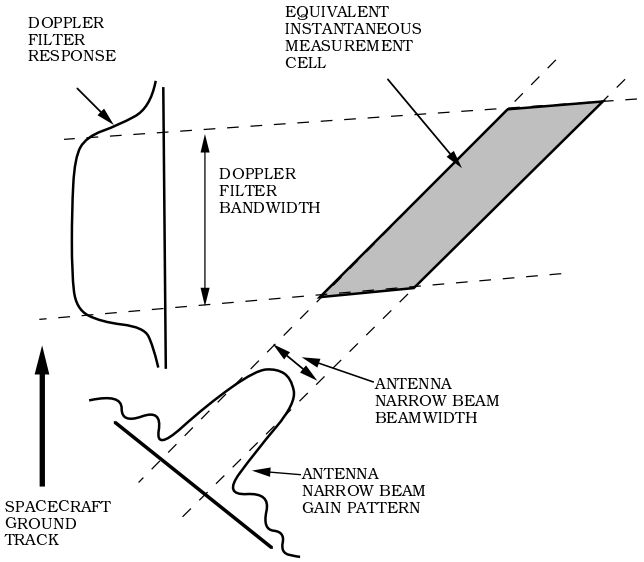

Figure 2.4: *NSCAT cell geometry.*

[14] used NSCAT data in another study to determine Arctic sea ice extent and melt onset. Drinkwater and Liu [15] monitored sea ice motion in the Antarctic and the Arctic using a combination of NSCAT reconstructed imagery and wavelet analysis.

Due to catastrophic solar panel failure the NSCAT mission only lasted about 10 months. Still, NSCAT has been a valuable tool in many land and ice studies as it has proven its sensitivity to critical surface parameters.

2.1.4 The SeaWinds Scatterometer on QuikSCAT

As a result of the premature end of the NSCAT mission due to the power failure on the ADEOS-1 satellite, QuikSCAT was launched as a "quick recovery" mission to help fill the gap created. QuickSCAT was launched on June 19, 1999. A similar SeaWinds scatterometer will fly on the ADEOS-II mission.

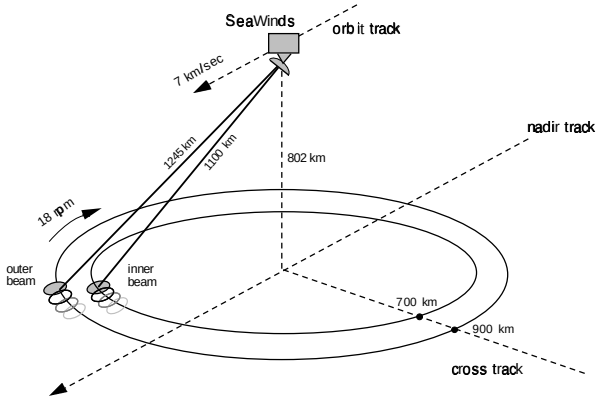

Figure 2.5: *SeaWinds measurement collection configuration.*

The SeaWinds instrument measures backscatter in much the same way as NSCAT. However it has a significantly different design than the fan-beam scatterometers flown on SASS and NSCAT. QuickSCAT uses a 1-meter parabolic antenna dish with two offset feeds for vertical and horizontal polarization. The antenna spins at a rate of 18 rpm and two pencil-beam footprint paths are scanned at incident angles of 46 degrees (H-pol) and 52 degrees (V-pol) as shown in Figure 2.5 and in Figure 2.6. The radar pulse is modulated and the received pulse is passed through a FFT to provide sub-footprint range resolution after it goes through Doppler compensation. The range resolution is set at 6 km. The pulse repetition frequency can also be controlled, and it set at 187.5 Hz. One hundred pulses of data are contained in each telemetry frame, and both signal and noise measurements are returned for each of the 12 sub-footprints called "slices". When the data is processed, each pulse "egg" and "slice" centroids are located and the σ^0 values are then computed for the "egg" and the best 3 of 12 "slices".

Like NSCAT, QuikSCAT generates an internal calibration pulse and load pulse every half-scan of the antenna. The pulses are then averaged to give the current gain

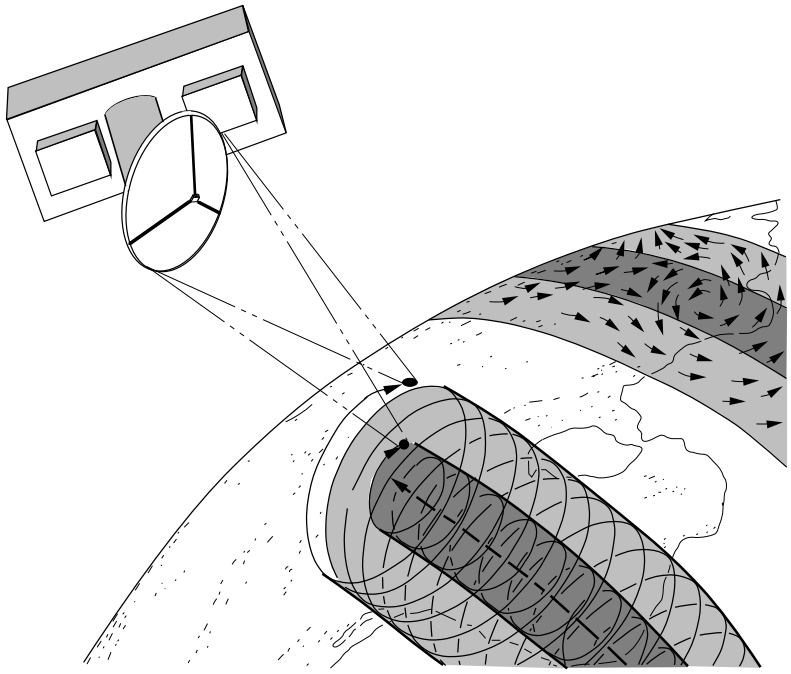

Figure 2.6: *SeaWinds scan pattern showing helixes traced by inner beam (light shade) and outer beam (dark shade) as spacecraft orbits.*

calibrations needed to convert the telemetry data into power measurements for the σ^0 calculation.

Even though the NSCAT and QuikSCAT instruments are similar, there are some significant differences. For a comparison of various parameters for NSCAT, SeaWinds, and other scatterometers see Figure 2.7. Because SeaWinds uses a compact dish antenna rather than multiple fan-beam antennas, the instrument is accommodated on the spacecraft more easily than many previous instruments. The SeaWinds swath is about 1800 km wide, which allows ocean wind measurements to be taken more frequently. The wider swath also improves temporal and spatial resolution in comparison with other sensors [16]. The SeaWinds instrument covers approximately 90% of the earth's surface and 100% of the polar regions each day. In comparison,

NSCAT requires 2-3 days to obtain complete coverage. As a result SeaWinds reconstructed imagery is less subject to blurring caused by sea ice motion. The SeaWinds σ^0 measurement variance is reduced by modulating the transmit pulse [17]. A detailed description of the types of image products created from QuikSCAT data is discussed in Chapter 4.

	SASS	ERS-1/2	NSCAT	SeaWinds
FREQUENCY	14.6 GHz	5.3 GHz	13.995 GHz	13.6 GHz
AZIMUTHS	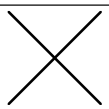	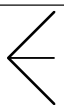	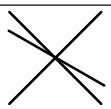	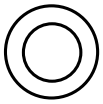
POLAR.	V-H, V-H	V ONLY	V, V-H, V	V-OUTER/H-INNER
BEAM RESOLUTION	FIXED DOPPLER	RANGE GATE	VARIABLE DOPPLER	PENCIL-BEAM
SCI. MODES	MANY	SAR, WIND	WIND ONLY	WIND/HI-RES
RESOLUTION	50/100 km	25/50 km	25/50 km	25 km/6x25km
SWATH	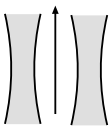	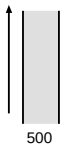 500	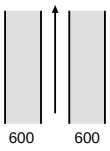 600 600	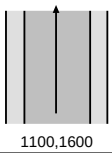 1100,1600
INCIDENCE ANGS	0° - 70°	20° - 70°	17° - 62°	42° & 54°
DAILY COVERAGE	VARIABLE	< 41 %	78 %	92 %
DATES	6/78 – 10/78	92–96 & 96–	8/96 – 6/97	5/99 – & 11/00

Figure 2.7: *Comparison of various parameters for SASS, ERS-1/2, NSCAT, and SeaWinds.*

2.2 Passive Microwave Remote Sensing

Microwave radiometers are passive instruments that observe natural microwave emissions of the earth's surface. Radiometers measure the brightness temperature, T_b, which is a function of surface temperature, T_s, and the emissivity of the surface, e,

$$T_b = eT_s. \tag{2.3}$$

The Rayleigh-Jeans approximation to Planck's Law of Thermal Radiative Emission is used to derive this proportional relationship [2]. This approximation is valid in the microwave portion of the spectrum. For a black-body, $T_b = T_s$, and the emissivity relates the amount of radiation emitted as compared to a black-body radiator. The emissivity, like σ^0, is a function of instrument and surface dependent parameters. Sensor frequency, polarization, incidence angle, and beam width are important. Emissivity is dependent on sea ice characteristics. The emissivity increases with water content. Also there is a higher emissivity with a higher salinity content due to the presence of brine. Snow accumulation rates also influence the emissivity.

Passive radiometers, like scatterometers, have proven a valuable tool for monitoring the polar regions of the earth. Several difference spaceborne radiometers are described below.

2.2.1 Early Radiometers (ESMR and SMMR)

The Electrically Scanning Microwave Radiometer (ESMR) was one of the earliest satellite microwave radiometers. Operating at 19.35 GHz this horizontally polarized radiometer flew aboard the Nimbus 5 platform from late 1972 to late 1982 [1]. ESMR had a swath width of 3,000 km and complete coverage of the polar regions were achieved in a single day, though due to frequent down times this requirement was often raised to three days.

ESMR data provided one of the first tools for detecting sea ice concentration [18]. There was very little contrast in sea ice observations at 19.35 GHz. Contrast between younger and older ice types was significantly improved with a newer version of ESMR aboard the Nimbus 6 satellite which used a 37 GHz frequency. However resolution was limited due to the noise caused by the electrical scanning configuration of the instrument.

Because of the knowledge gained from the ESMR instruments, second generation passive microwave radiometers were developed. The Scanning Multichannel Microwave Radiometer (SMMR) was one such instrument. SMMR was launched in 1978 aboard the Seasat satellite and collected dual-polarization measurements at

five different frequencies: 6.63, 10.69, 18, 21, and 37 GHz. The 21 Ghz channel was primarily used for atmospheric corrections due to its sensitivity to the presence of atmospheric water vapor. SMMR was initially designed to measure sea surface temperatures and wind speeds (not direction). However because of its multispectral nature SMMR became a useful tool for studying sea ice.

2.2.2 The Special Sensor Microwave Imager (SSM/I)

The Special Sensor Microwave Imager (SSM/I) aboard the Defence Meteorological Satellite Program series of satellites is another imaging microwave radiometer. SSM/I is a total-power, seven channel, four-frequency radiometer. The satellite is a polar orbiting, sun-synchronous instrument at a height of 843-877 km from the surface of the earth. The channels are vertical and horizontal polarizations at 19.35, 37.0, and 85.5 GHz and vertical polarization at 22.235 GHz (See Table 2.1). An integrate-and-dump filter is used to make the Radiometric brightness-temperature measurements [21]. The 3-dB footprints vary from 15-70 km in the cross-scan direction and 13-43 km in the along-scan direction (See Table 2.1). The antenna beam intersects the Earth's surface at an incidence angle of 53.1 degrees (as measured from the local Earth normal) as shown in Figure 2.8. This results in a 1417-1481 km wide swath on the surface of the earth.

The SSM/I antenna is a conical scanning, parabolic reflector with dimensions of 0.6 meters by 0.7 meters. It is fed by a corrugated, broad-band, seven-port horn antenna. The parabolic antenna rotates at 31.6 RPM and has a scan period of 1.899 seconds. The instrument samples through 102 degrees for each scanning revolution. Each of the 85 GHz channels scan continuously, while the 19, 22, and 37 GHz channels sample every other interval of every other scan. An A-scan is the scan on which all channels are sampled. The 85 GHz-only scan is called the B-scan. The A and B scans denote a scan-pair. Because of these sampling characteristics, there are 128 high frequency (85 GHz) samples and 64 low frequency (19, 22, or 37 GHz) samples in each A-scan. There are one-fourth as many elements in a low frequency (19, 22, or 37 GHz) swath than in a high frequency (85 GHz) swath.

Table 2.1: *Sizes of the 3-dB Antenna Footprints of the SSM/I Channels. The Approximate Spacing of the Measurements in the Cross-Track and Along-Track Directions (i.e. The Spatial Sampling Density) Is Also Shown.*

SSM/I Chan			3 dB Ftprint (km)		Approx
Chan	Freq (GHz)	Pol	Along	Cross	Spc (km)
1	19.35	V	69	43	25
2	19.35	H	69	43	25
3	22.235	V	50	40	25
4	37.0	V	37	28	25
5	37.0	H	37	29	25
6	85.5	V	15	13	12.5
7	85.5	H	15	13	12.5

The orbital period for the satellite is about 102 minutes. The SSM/I orbits the earth about 14.1 times per day. The processing breaks the data streams into passes. A pass is a pole-to-pole swath which is either ascending (south to north) or descending (north to south). A complete pass contains about 51 minutes of data or about 1610 A and B scans.

A small mirror reflecting cold sky radiation into the feed and a hot reference absorber are mounted on the device to provide calibration references for the SSM/I radiometer. This scheme provides an overall absolute calibration every 1.9 seconds.

Before converting the antenna temperatures to brightness temperatures, corrections are made for two types of systematic errors. The first error is due to the feed-horn partially seeing the cold-space reflector at the edge of the Earth-viewing portion of the scan. The second error is the mean difference between the SSM/I antenna temperature observations and the Wentz radiative transfer model for the ocean and intervening atmosphere.

The brightness temperatures measured by the SSM/I are a combination of the effective brightness temperature of the Earth's surface and the emission, scattering, and attenuation of the atmosphere. Surface brightness is a function of the properties of the soil and overlaying vegetation and their physical temperatures. The most

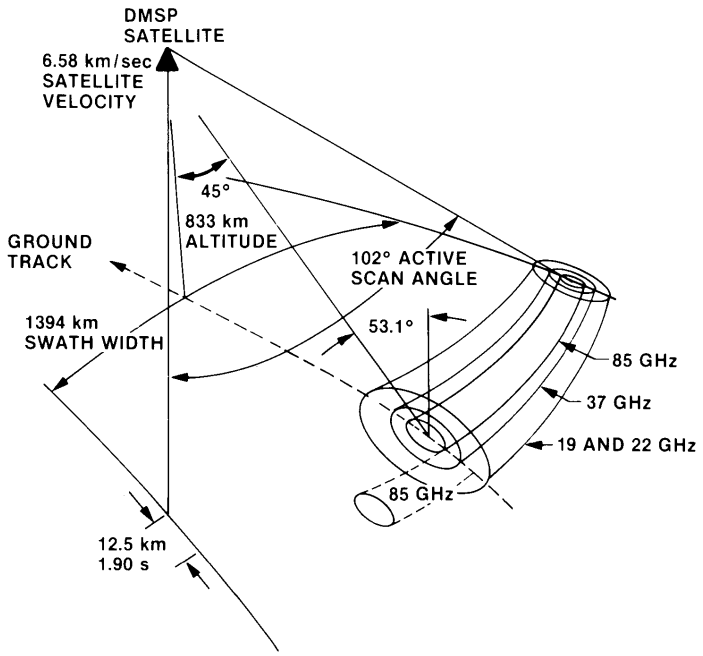

Figure 2.8: *SSM/I scanning measurement geometry [1].*

important factors affecting a radiometric measurement are the surface emissivity and temperature, the vegetation canopy (if applicable), the viewing angle, and the atmospheric conditions. Due to the variability of brightness temperatures, large icebergs radiate a different T_b measurement than the surrounding sea-ice or ocean. Therefore, we can use SSM/I's images from each of its seven channels to track relatively large antarctic icebergs.

If the effects of the atmosphere are ignored, an SSM/I measurement can be modeled as a product of the surface brightness and the antenna pattern. The ith measurement Ta(i) (in K) is obtained by integrating the product of the surface brightness response $T_b(x,y)$ (in K) and the antenna at the surface $G_i(x,y)$

$$T_a(i) = \overline{G}_i^{-1} \int\int G_i(x,y) T_b(x,y) dxdy \tag{2.4}$$

where

$$\overline{G}_i = \int\int G_i(x,y) dxdy \tag{2.5}$$

where integrals over the surface area correspond to the non-negligible gain of the antenna. The antenna pattern acts as a spatial low-pass filter of the surface brightness, limiting the effective resolution of the measurement.

SSM/I data sets offer improvements over previous spaceborne radiometers in sea ice studies. With the SSM/I instrument geolocation in improved. The estimation of total sea ice concentration in both the Arctic and Antarctic regimes are calculated by the NASA Team algorithm with the use of SSM/I polarization and gradient ratios computed from the 19 and 37 GHz channels [22]. In [23] and [24] SSM/I resolution enhancements are considered.

2.3 Resolution Enhancement

The resolutions of many of the images discussed are sufficient for studying many large scale phenomena such as surface winds yet the resolution is too low for many other studies. In order to improve the resolution the Scatterometer Image Reconstruction (SIR) algorithm is used to enhance the spatial resolution [23]. SIR is an iterative block multiplicative algebraic reconstruction technique that uses multiple passes of the satellite to improve the resolution of reconstructed imagery. SIR increases the spatial resolution with the help of the increased sampling which raises the side lobes of the antenna pattern in the spatial frequency domain.

Images of the A and B parameters are created with the SIR algorithm for scatterometers. NSCAT images are recreated with the SIR with Filtering (SIRF) algorithm [25] that includes a median filter. Reconstructed NSCAT images have an effective resolution of 8-10 km and are created on a 4.45 x 4.45 km grid. The median filter is not used with ERS-1/2 data. ERS-1/2 reconstructed images have an effective resolution of 20-25 km and are created on a 8.9 x 8.9 km grid. Reconstructed images are also created with SeaWinds data yet due to a fixed-incidence angle the parameter B cannot be estimated. The egg data sets have a 4.45 km pixel resolution with an effective surface feature resolution of 8-10 km. Slice reconstructed imagery currently has the highest resolution for scatterometers with a 2.225 km pixel resolution and a 4-5 km effective resolution.

Examples of NSCAT A_v and B_v images of the world are shown in Figure 2.9. These images are not displayed in full resolution but still show variations in parameters over land and ice surfaces. Desert regions such as the Sahara Desert exhibit the lowest areas of backscatter while areas like the Amazon and Central Africa rain forests have significantly higher A_v values. The glacial ice areas of Greenland and Antarctica have the highest backscatter values. The B_v image is noisier than the A_v image but it also contains important information about land and ice surfaces. The B_v images are very similar to A_v images with the values in the desert being low due to a σ^0 fall-off with increasing incidence angle. The values in the rain forest and ice remain high due to volume scattering.

With radiometer data such as SSM/I a univariate form of the SIR algorithm can be applied. Resolution enhancement is more difficult with SSM/I data due to it's low side lobes. Yet, there is a clear improvement of resolution with the SIR algorithm. SSM/I brightness temperature SIR images have an 8.9 km pixel resolution for all channels except 85V and 85H which have a pixel resolution of 4.45 km.

The SIR allows a comparison of reconstructed images with similar resolution. Though resolution is improved, ice motion during the imaging period can present a concern. In a six day period, for example, icebergs and sea ice can move tens of kilometers. This can represent several pixels in the reconstructed image. The result is a reconstructed image that represents an average surface response. However for most of the image data sets used in this study this does not significantly affect the ability to track icebergs.

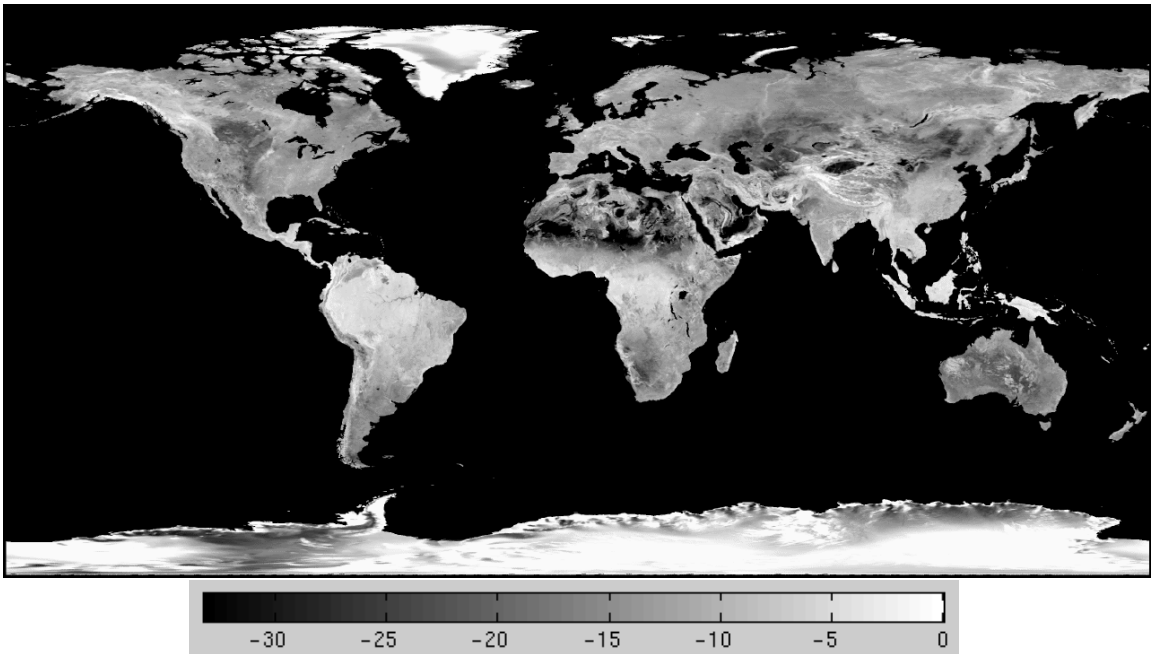

a) A_v Image with a grey scale.

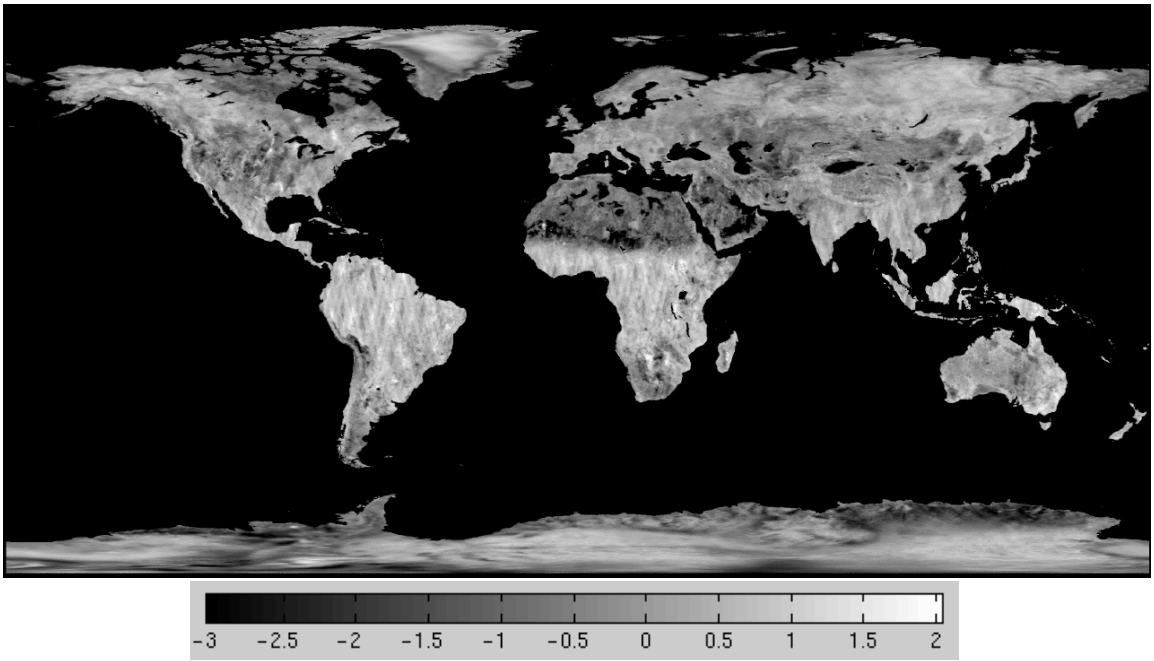

b) B_v Image with a grey scale.

Figure 2.9: *Sample NSCAT a) A_v and b) B_v SIRF images of the world. The original image has a greater spatial resolution than can be displayed. Ocean pixels have been masked out of the image.*

Chapter 3

Using Passive Radiometer Data to Track Icebergs

The Antarctic continent continually releases glacial ice into the ocean in the form of icebergs calving from glaciers and ice shelves. Microwave radiometers provide information on the temporal and spatial behavior of large Antarctic icebergs. In this report, results are presented from the observation of several icebergs during 1999-2000 using the Defence Meteorological Satellite Program's (DMSP) radiometer (SSM/I). The SSM/I images are evaluated for their usefulness in tracking these icebergs. Multi-channel analysis shows a tradeoff between high resolution and low resolution images.

3.1 Introduction

Microwave radiometers, such as the Special Sensor Microwave/Imager (SSM/I), have multiple applications in remote sensing over the ocean. Radiometers, for example, provide essential information for numerical weather-prediction models.

SSM/I data has also been used for land and ice studies, including snow-cover classification, measurements of soil and plant moisture content, atmospheric moisture over land, land surface temperature, and polar ice mapping. However, the relatively low resolution of SSM/I limits its use in land and ice studies. The resolution of the SSM/I is determined by its antenna-beam pattern with the resolution varying from approximately 13 to 69 km. To reduce this limitation, resolution-enhancement algorithms are applied to the data. Resolution enhanced images are then used to monitor and track the spatial and temporal movements of Antarctic icebergs.

This chapter is organized as follows: Section 2 provides a detailed description of using the SSM/I to track Antarctic icebergs. Each of the seven SSM/I channels

is used to track a series of large icebergs. In Sections 3 and 4 comparisons are made between each channel's ability to track the icebergs. Finally conclusions are made in the last section.

3.2 Tracking Icebergs

Some factors involved in tracking Antarctic icebergs are resolution, atmospheric disturbance, contrast with sea-ice, contrast with land, contrast with ice shelves, and T_b blending with ice shelves and other icebergs. This reports examines most of these factors as they relate to tracking icebergs.

Image resolution is a very important factor for tracking Antarctic icebergs. For each SSM/I operation frequency there is a different corresponding footprint size. The footprint size is determined by the antenna's beamwidth. For a circular aperture, the half power beamwidth in radians is approximately the wavelength divided by the antenna's diameter. With higher frequencies the beamwidth narrows, and we generally get better spatial resolution.

The image resolution is also enhanced using the BYU-MERS SIR algorithm [23]. The SIR algorithm is a "reconstruction" algorithm, which attempts to reconstruct the underlying brightness distribution (T_b) on a high-resolution grid (see Fig. 3.1) from the lower-resolution measurements (T_a). The SIR algorithm provides improved resolution at the expense of an increased noise level in the images.

There is a significant tradeoff between frequency channels. As Figure 3.2 illustrates, as the frequency increases there is more signal attenuation in the atmosphere. Precipitation and clouds significantly add to the atmospheric distortions. There are absorption bands due to water vapor and oxygen at frequencies near 22, 58, 120, and 180 GHz. As Figure 3.3 illustrates, higher frequencies correspond to higher extinction (or power attenuation) coefficients due to clouds. Precipitation also has a similar effect. When using radiometer T_b images to track icebergs this result is especially significant. While lower frequency images have a lower spatial resolution they are generally less noisy. Higher frequency images have much better spatial resolution but are much more sensitive to atmospheric disturbances. The images are therefore noisy

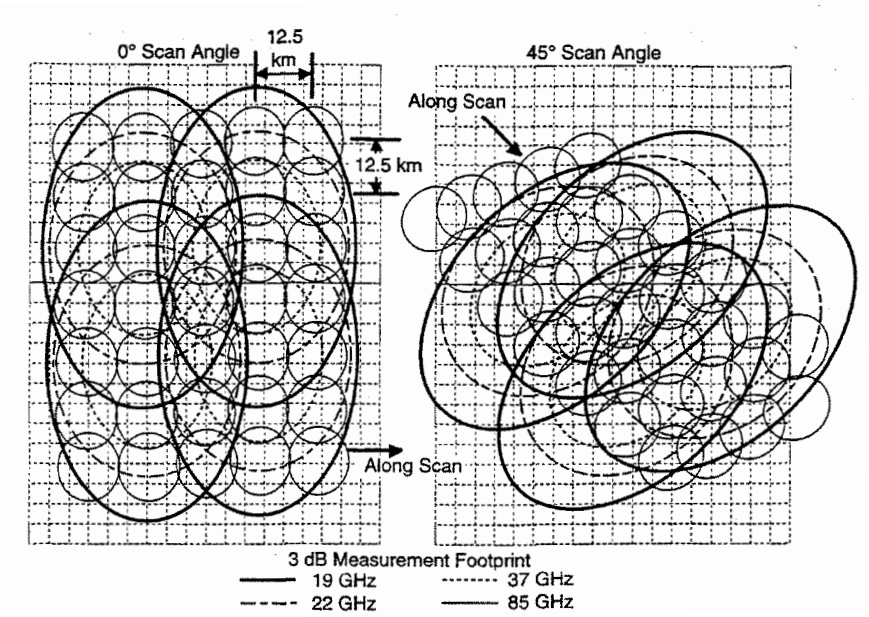

Figure 3.1: *The locations of the measurement footprints for several along-track measurements for two scans are illustrated for two different scan locations. [2]*

and cause a distortion in contrast between icebergs and sea-ice (or ocean), making it more difficult to track icebergs (see Figure 3.4 for an example of the different types of SSM/I images). Because of noisy images, icebergs cycle through periods of being visible and then not being visible.

There are tradeoffs to using high and low resolution images. A higher resolution image affords us the ability to resolve individual icebergs from each other and their surroundings. An example of this is observed with icebergs b15a, b15b, and b15c (See Fig 3.5). The advantage of using lower resolution images is a clearer and more consistent image. For example iceberg a23a is visible for 91.1 percent of the images for channel one but only visible 29.6 percent of the time with channel 7 (See Table 3.1). Also, icebergs such as a35a appear larger with the low frequency channels due to a larger antenna footprint size.

Some icebergs are difficult to detect because of their location. For example, icebergs such as b09a, a38a, and a38b are difficult to detect due to their proximity

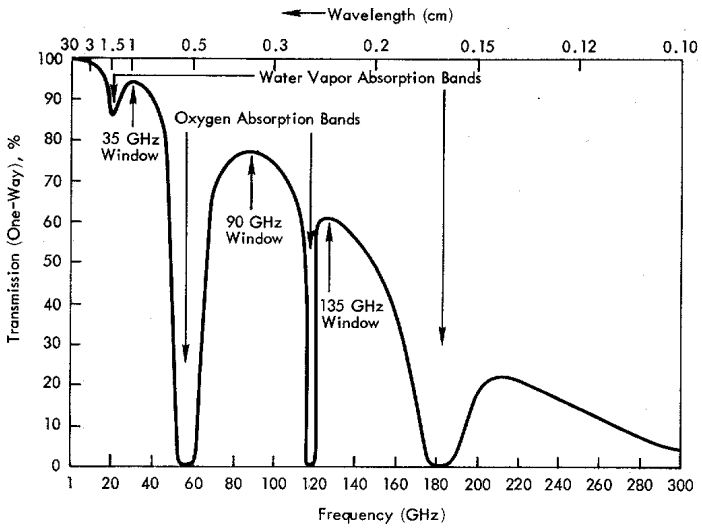

Figure 3.2: *Percentage transmission through the earth's atmosphere, along the vertical direction, under clear sky conditions. [2]*

to the Antarctic continent. The T_b values of these icebergs tend to blend with the T_b values of the Antarctic continent. This is especially true for lower resolution images.

The different T_b values of icebergs and sea ice play an important role in tracking icebergs. The T_b values of the sea ice are generally much higher than the T_b values of the icebergs. The T_b values of the sea ice vary according to sea ice type. Multi-year ice tends to have lower (darker) T_b values and first year ice has higher T_b values. This presents obstacles to tracking icebergs in different regions. For example, icebergs in the Weddell sea surrounded by dark multi-year ice tend to be more difficult to track due to relatively low contrast with the sea ice. Icebergs in the Ross sea, surrounded by bright first year ice, are easier to track due to higher contrast with their surroundings. Icebergs located fairly close to the Ronne and Ross ice shelves are easiest to track. This is due to the consistent T_b values of the sea ice that forms just off these ice shelves.

Icebergs located between 180 degrees East longitude and 0 degrees longitude seem easier to track with low resolution images than with noisier higher resolution

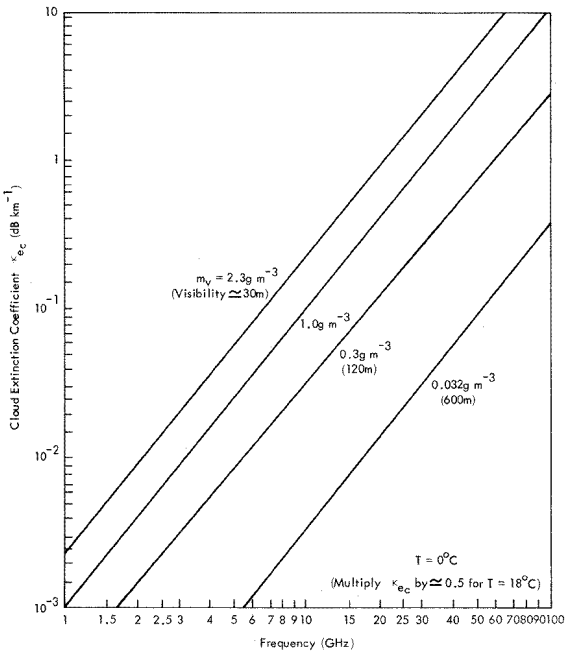

Figure 3.3: *Extinction coefficient of clouds or fog for several water contents (and corresponding visibilities) at 0 degrees Celsius. [2]*

images. This is due to the consistency in contrast between the iceberg and its surroundings. These icebergs tend to be difficult to resolve with surrounding ice shelves and they tend to blend together. The smaller icebergs in this region are particularly difficult to track because of this. The best time of the year to track these icebergs, as well all the other icebergs, is during the Antarctic spring in the months of August through October.

3.3 Results and Distributions

From July 1999 to October 2000, 31 Antarctic icebergs are tracked and monitored using enhanced resolution SSM/I images. Each iceberg is tracked for its life span (See Table 3.1). The iceberg positions, and T_b values are recorded along with the average T_b value of the surrounding sea-ice or ocean sea water. These T_b values are then studied to find useful patterns for future iceberg tracking.

The T_b distributions for each channel are studied and the results are instructive. Maximum T_b values for each of the radiometer images and for each channel are calculated and plotted. The mean T_b value for these maximum values increases as the channels frequency increases. The average T_b value for each iceberg and for each channel also increases with increasing channel frequency. This is consistent with the Plank Radiation-Law curves and can be expected. However, T_b values are very different depending on the polarization used. Figure 3.6 shows the iceberg temperature brightness distributions for each channel. The mean T_b values of the horizontally polarized channels are clearly lower than the vertically polarized channels. The reason for this is not exactly known. We do know that radiation from the atmosphere is randomly polarized (unpolarized), where the emissions from the surface are usually polarization-dependent.

The polarization dependence of the surface seems closely related to the emissivity. The emissivity is (Equation 2.3 repeated here for convenience)

$$e = T_b/T \tag{3.1}$$

where T_b is the brightness temperature and T is the physical temperature of the material. If we assume the physical temperature is constant at 0 degrees Celsius or 273 K, then we can approximate the average emissivity of each channel by dividing the average T_b value by 273 K (See Table 3.2). The average emissivity due to vertical polarization is higher than that due to horizontal polarization. The distribution of the emissivity would also be similar to the T_b distributions (See Figure 3.6). The average emissivity for the vertically polarized channels is roughly 0.8 while the average emissivity for the horizontally polarized channels is about 0.7. The exception is channel 7 (h-pol or v-pol) which has a slightly higher average emissivity.

The reason for the variation in emissivity and average brightness temperature is the physical properties of the iceberg. We know that the T_b values are inversely proportional to the normalized radar backscatter values. Vertically polarized signals are more sensitive to vertically oriented objects, such as trees, and horizontally polarized signals are more sensitive and give a stronger backscatter to horizontally oriented

objects. It has been observed that in scatterometer images, icebergs usually have a higher normalized backscatter with horizontal polarization and therefore a lower T_b value.

The T_b distributions shown in Fig 3.6 clearly show a Gaussian distribution with different means but similar variances. The exceptions to this are channels 2 and 5 which have slightly higher variances. There may be several reasons why channels 2 and 5 have higher variances. For one, we do observe "tails" extending to the left of most of the distributions. The temperature brightness values in these tails most likely correspond to the summer ice melt. During an Antarctic summer the physical temperature rises and melts the surface of the iceberg. This surface melt water emits a much lower T_b value. Channels 1, 2, and 5 seem to be most sensitive to this change. Channels 6 and 7 (85 GHz) do not seem to show this tail effect. This is probably due to the randomness in the atmospheric distortions. We can also see this tailing effect by plotting the T_b distributions of the surrounding sea-ice or ocean sea-water (See Figure 3.7). These tails are more pronounced due to the fact that every Antarctic summer most of the sea-ice melts and the resulting T_b values come from the sea-water which has a lower emissivity (Lower T_b). Again we see that channels 1, 2, and 5 are more sensitive to this effect and that channels 6 and 7 are not. The result of this tailing effect might be very useful for future studies of the Antarctic summer ice-melt.

The T_b distribution for an individual iceberg varies but the general observations given above apply (see Fig. 3.8). When plotting each iceberg's T_b values for each channel as a function of time, several patterns are observed. When the iceberg is located in the Antarctic sea-ice it appears darker in contrast than it's surroundings. When icebergs such as b10a, a22b, or d11 move out of the sea-ice they normally appear brighter than the surrounding ocean. The sea-ice usually has brighter T_b values than the iceberg while the iceberg usually has brighter T_b values than ocean water. The channels clearly show a drop in the T_b values during the Antarctic summer months due to the change in physical temperature. These facts are very useful when tracking icebergs.

3.4 Detection

A percentage measure for the ability to track each iceberg was determined for each channel and are shown in Table 3.1. Each percentage represents the number of days the iceberg was visible of all days attempted. Before this study, it was assumed that the higher frequency (higher resolution) channels would be the best for tracking icebergs. However, the results did not turn out as expected. Even though the higher frequencies channels provide a better resolution image, they are much noisier due to atmospheric disturbances. In general the lower frequency channels are more useful for tracking relatively large Antarctic icebergs. There were a few exceptions. Icebergs such as a43a, a43b, and a43c are tracked just as easily with low frequency channels as with high frequency channels. This is due to the iceberg's relatively large size and to the fact that these icebergs are located near the Ronne ice shelf where the image is not as noisy. There are a few cases were smaller icebergs such as c016 are better tracked with high frequency (higher resolution) channels. The very best channels for tracking icebergs seem to be the lower frequency (19, 22 GHz) channels.

3.5 Conclusion

In this chapter seven SSM/I frequency channels are evaluated for tracking several Antarctic icebergs. While higher frequency channels provide a better resolution image than low frequency channels, they are noisier due to the high frequency sensitivity of atmospheric distortions. Lower frequency channels provide lower resolution images but are not as noisy.

Differences in T_b distributions for each frequency channel are due to differences in sensitivity to summer ice melt and to differences in emissivity for horizontally and vertically polarized images. Iceberg T_b values are generally lower than sea-ice T_b values due to the physical characteristics of each type of ice.

Percentages for the ability to track each iceberg are determined. The lower frequency (lower resolution) images are determined to be the best for tracking Antarctic icebergs. In a few cases the higher frequency images are more useful for tracking smaller icebergs.

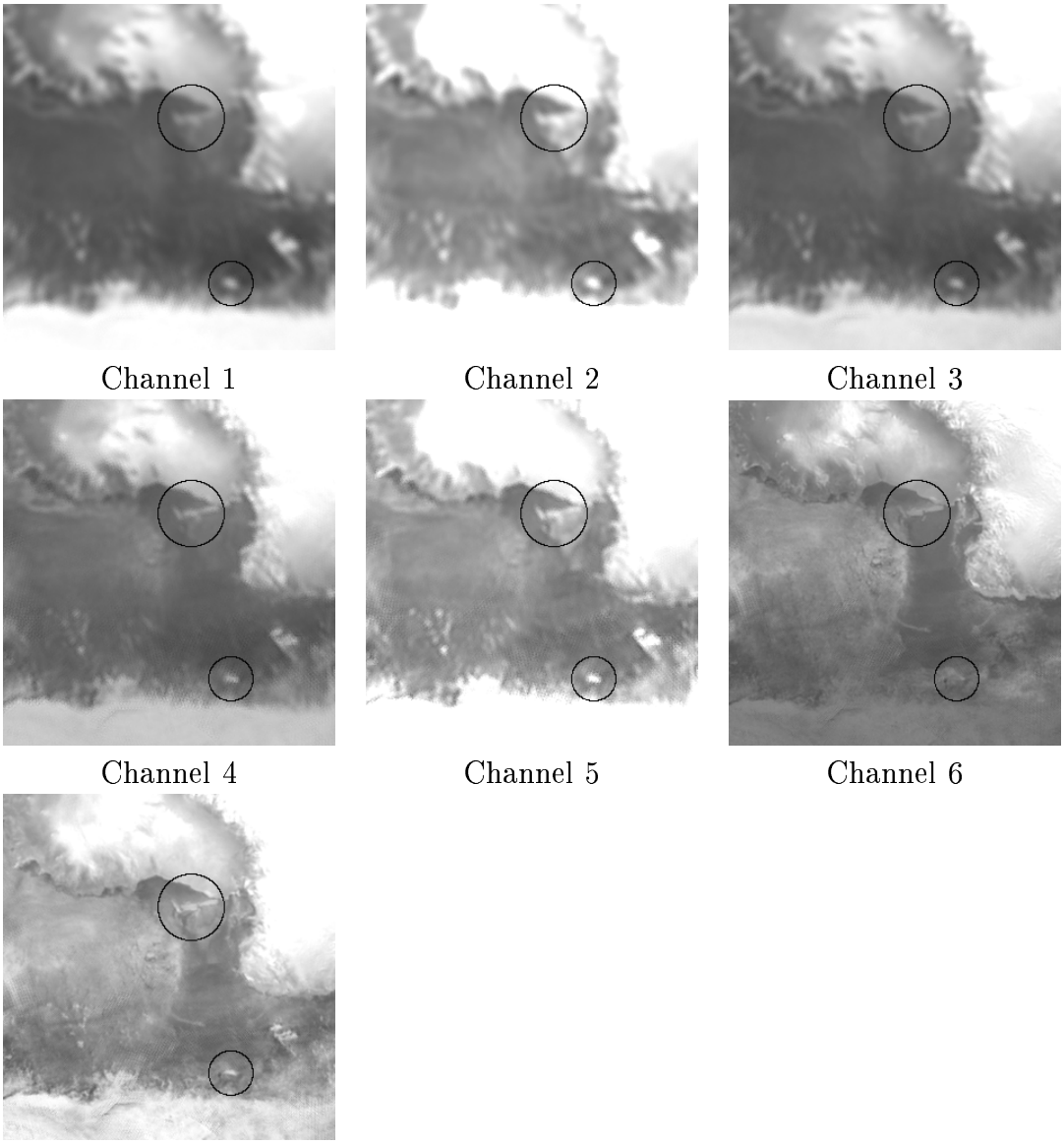

Figure 3.4: *Seven images of the seven SSM/I channels (Julian Day 204). Several icebergs are indicated. The bright area at the top is the Antarctic continent. The Dark Center area is sea ice. Lower region is open ocean. See Figure 3.5c for a* T_b *gray scale.*

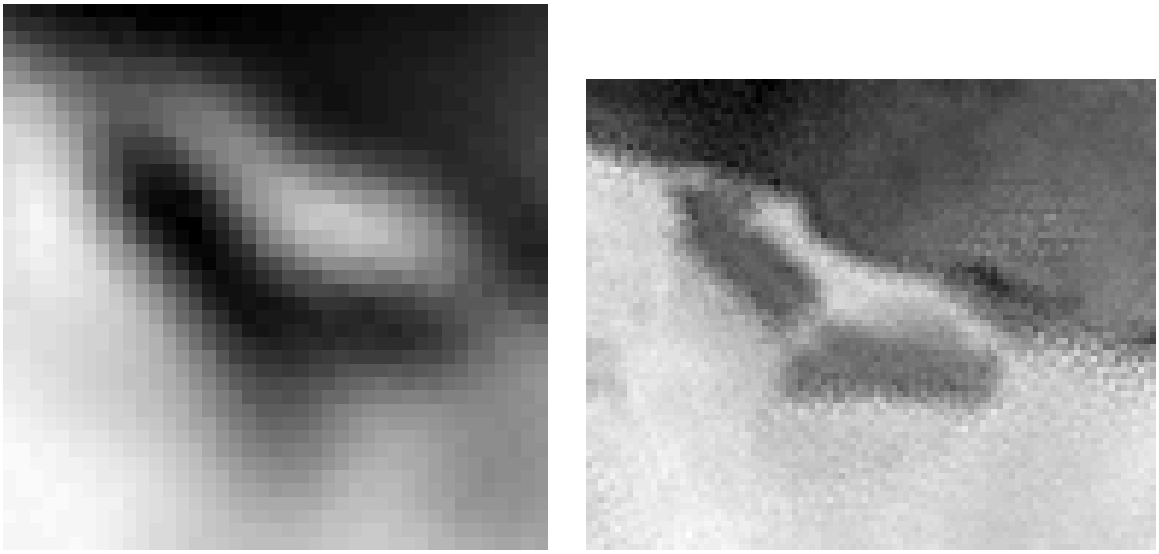

a) Channel 1 (v-pol 19GHz)

b) Channel 7 (h-pol 85GHz)

c) T_b

Figure 3.5: *Image of icebergs b15a, b15b, and b15c for a) SSM/I channel 1 and b) channel 7. The sea ice appears white, while the icebergs and ice shelf appear dark. Gray scale shows scale of T_b values.*

Table 3.1: *Percentages for ability to track each iceberg using each channel.*

Iceberg	Number of Days Tracked	Channel						
		1	2	3	4	5	6	7
a044	180	100	100	98.8	98.8	100	86	96.3
a22a	449	97.1	88.2	90.6	90.2	85.3	64.8	59.2
a22b	264	84.1	78.4	83.7	67.8	65.2	53.4	45.1
a22c	418	34.2	32.3	34	22.5	22	30.9	24.9
a23a	450	91.1	89.1	87.1	64.7	74	31.6	29.6
a23b	110	55.6	39.1	51	19.1	32.7	7.3	15.5
a35a	400	46.9	58.1	50.4	10.3	22.8	18	09.8
a35b	140	12.4	35	42.3	33.6	29.2	2.2	1.5
a35c	140	9.3	17.9	3.6	5.7	5.7	7.1	5
a38a	286	82.9	80.8	80.4	76.6	84.6	26.2	9.1
a38b	424	96.2	94.6	92.7	62.7	86.3	21	15.1
a43a	165	95.8	95.8	95.8	100	100	90.9	87.9
a43b	165	95.2	98.2	98.2	100	100	78.8	89.7
a43c	151	100	100	100	100	100	82.1	82.8
b014	431	70.3	75.9	72.6	63.1	68	31.8	18.8
b015	15	40.0	86.7	66.7	93.3	46.7	100	100
b016	201	28.4	26.4	12.9	45.3	54.7	30.3	38.8
b017	166	68.7	80.1	62	85.5	89.2	62	75.9
b018	42	0	0	0	9.5	7.1	21.4	40.5
b019	42	0	0	0	9.5	7.1	0	0
b09a	449	53.7	46.3	53	57.7	51.9	42.1	40.1
b09b	449	87.1	63.9	64.1	30.7	46.1	2.9	1.6
b10a	167	79.6	87.4	74.9	68.3	70.1	73.7	40.1
b15a	171	90.6	62	86	100	91.2	91.8	91.8
b15b	172	51.2	39.5	77.3	88.4	87.8	98.8	71.5
b15c	46	71.7	82.6	87	97.8	100	100	100
b15e	53	13.2	7.5	17	22.6	18.9	32.1	11.3
c010	445	79.6	60.7	42	48.8	38.2	7.9	1.8
c016	41	26.8	0	7.3	68.3	36.6	53.7	51.2
d011	398	49.2	39.2	37.2	22.9	31.4	54.8	23.1
d015	448	75	39.7	28.3	42.4	36.6	21	6.3
TOTAL	7478	69.6	63.6	62.2	55.8	58.6	39.2	32.4

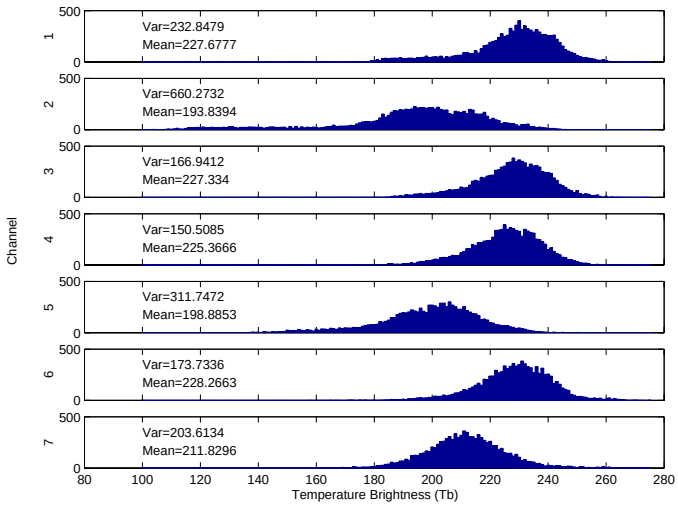

Figure 3.6: *T_b distribution for all iceberg brightness temperatures recorded for every iceberg and for every channel for approximately one year.*

Table 3.2: *Average iceberg emissivity for each SSM/I channel with an approximate physical temperature of 273 K.*

Chan	Freq (GHz)	Pol	Ave T_b	T	Emis
1	19.35	V	227.7	273	0.834
2	19.35	H	193.8	273	0.710
3	22.235	V	227.3	273	0.833
4	37.0	V	225.4	273	0.826
5	37.0	H	198.9	273	0.729
6	85.5	V	228.3	273	0.836
7	85.5	H	211.8	273	0.776

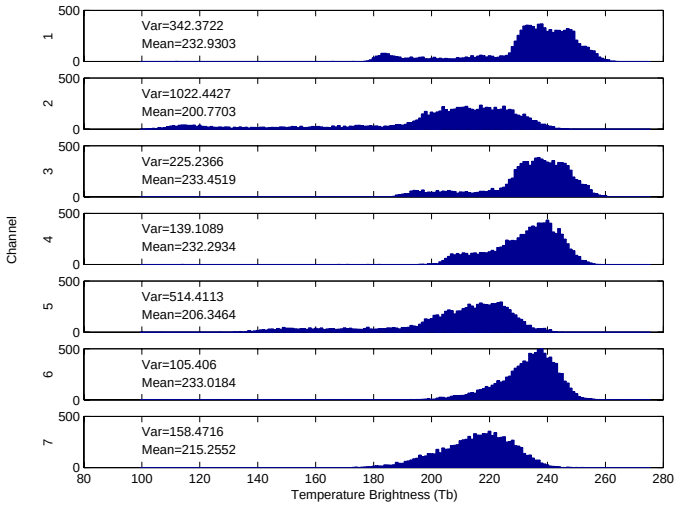

Figure 3.7: *T_b distribution for all sea-ice/ocean brightness temperatures recorded for every iceberg and for every channel for approximately one year.*

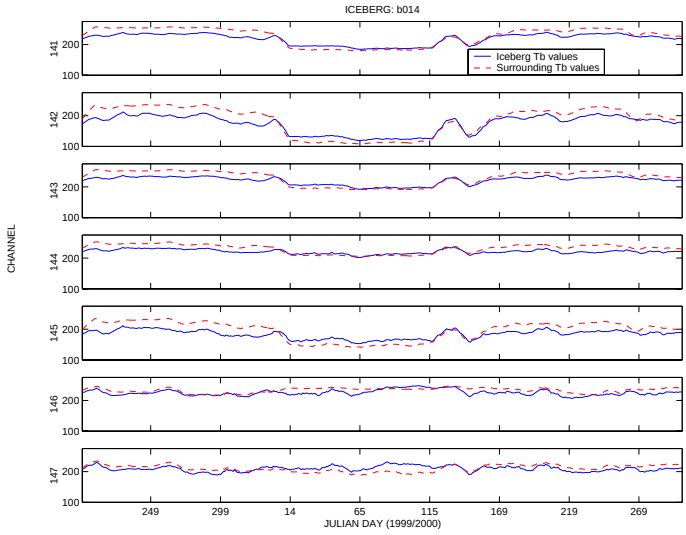

Figure 3.8: *T_b values for iceberg B14.*

Chapter 4

Utilizing QuikSCAT Data to Track and Monitor Antarctic Icebergs

Microwave scatterometers provide information on the temporal and spatial behavior of large antarctic icebergs. In this Chapter, results are presented from the observation of several icebergs during 2000 using the SeaWinds scatterometer on the QuikSCAT satellite (QSCAT). The QSCAT images are evaluated for their usefulness in tracking icebergs. Multi-image analysis shows the similarities and differences between the types of images produced. The QSCAT images are also useful for observing the effect of katabatic winds on icebergs and ice shelves.

4.1 Introduction

Using resolution enhanced QSCAT images several distinct features of the Antarctic continent can be seen. Figure 4.1 shows eight different types of images of the Weddell Sea produced using the SIR and AVE algorithms. Sea ice, ice shelves, and land features can be clearly seen as σ^0 values vary across the Earth's surface. Relatively large Antarctic icebergs can be readily identified as objects of high backscatter against the lower backscatter of sea ice or ocean.

In order to determine the feasibility and reliability of using QSCAT images for tracking antarctic icebergs a set of 14 different icebergs were tracked for approximately one year (the year of 2000) using eight different QSCAT image types (See Table 4.1). The icebergs were selected from different parts of the Antarctic continent to give a broad perspective on the ability to track icebergs in each area. Tradeoffs and advantages for using each image type will be addressed. In order to understand the

types of images used, this report will begin by describing differences between the various types of images produced.

The Antarctic katabatic winds play a major role in the motion of sea ice and icebergs. While tracking the 14 icebergs in Table 4.1 the effect of these winds can be seen. Knowing the relationship between these winds, icebergs, and ice shelves may play an important role understanding a larger system of global ocean currents which transport water, heat, and salt around the world.

Table 4.1: *Percentages for ability to track each iceberg using each type of image.*

Iceberg	Image Type							
	queh_ave	queh_sir	quev_ave	quev_sir	qush_ave	qush_sir	qusv_ave	qusv_sir
a22b	82.6	80.7	48.6	55.2	76.2	79.0	55.2	46.7
a22c	75.2	86.3	72.9	75.8	88.9	79.4	82.4	69.6
a35a	74.1	84.8	53.3	82.8	96.9	88.1	99.6	76.8
a38a	60.3	80.9	26.2	29.8	78.0	85.8	82.3	75.9
a38b	58.6	48.9	26.5	26.1	65.9	62.1	60.6	45.5
a43a	95.9	97.4	92.2	96.4	100	99.5	99.5	99.5
a43b	96.4	99.0	78.8	94.8	100	99.5	100	99.5
a43c	98.9	100	86.6	100	100	100	100	100
b09a	82.9	89.5	87.7	87.7	92.9	87.0	92.5	90.9
b014	86.3	91.9	79.5	82.9	93.5	92.8	88.7	87.3
b15e	64.9	73.7	57.9	78.9	86.0	70.2	84.2	73.7
b016	77.8	78.7	87.0	89.7	89.1	80.9	94.3	90.8
c016	46.4	72.5	37.7	62.3	56.5	63.8	82.6	79.7
d011	75.3	88.0	75.7	81.9	81.9	86.2	82.3	84.4
Average	78.6	84.5	68.9	76.4	88.0	85.2	86.8	81.0

4.2 Image Types

The BYU Microwave Earth Remote Sensing (MERS) Laboratory has developed a standard set of QSCAT land/ice images used in various land and ice studies [26]. A description of the standard set of QSCAT land/ice images used in this study is shown in Table 4.2. Each image type differs according to the polarization used and the method or algorithm used to process the image (See Figure 4.1 for samples of the

image types). All the images are measurements of the normalized radar backscatter values in dB. Each type of image is distinguished from other image types by a rather simple naming scheme. This section will describe this naming scheme and give a brief introduction to the types of images used in this study.

The first and second letters in the image name specify the origin and type of data used in creating the image. The name for each image type begins with the letter 'q' denoting the images come from the SeaWinds scatterometer on board the QSCAT satellite. The second letter 'u' signifies that data from both ascending and descending satellite passes are combined when creating the images. When combining ascending and descending passes of the satellite, we make the assumption that the surface remains the same.

Table 4.2: *The standard set of QSCAT land/ice images used in this study. All images use both ascending and descending data.*

Types of Images Produced			
Prefix - extension	Type	Polarization	Reconstruction Algorithm
queh - ave	egg	h	AVE
queh - sir	egg	h	SIR
quev - ave	egg	v	AVE
quev - sir	egg	v	SIR
qush - ave	slice	h	AVE
qush - sir	slice	h	SIR
qusv - ave	slice	v	AVE
qusv - sir	slice	v	SIR

The third letter in the image type name specifies whether the image σ^0 measurement are reported from 'eggs' (e) or 'slices' (s). These measurements differ in their spatial sizes and shapes. The QSCAT antenna footprint is elliptical. The measurement resolution can be further improved with on-board range-doppler processing. Using this filtering, 12 individual σ^0 measurements are obtained with each footprint,

though only 8 are reported in the distributed products. These individual measurements are termed 'slices'. Depending on the instrument mode and antenna beam, these slices are 4-6 km long by 20 km wide. The 'egg' measurements are the summed measurements of 8 center slices. Depending again on the antenna beam and instrument mode, the effective resolution and shape of the egg measurement is about 15 km by 25 km. Egg measurements have a lower resolution, but are less sensitive to calibration errors.

The fourth letter in the image type name is either 'h' for horizontal polarization or 'v' for vertical polarization. QSCAT makes σ^0 measurement from incidence angles of 46 degrees and 54.1 degrees corresponding to the inner and outer beams. The inner beam measurement is horizontal polarization while the outer beam is vertical polarization. Both horizontal and vertical polarization images are studied in Table 4.1.

The last three letters in the image type naming scheme specifies the type of reconstruction algorithm used. The 'SIR' images are products created using the Scatterometer Image Reconstruction (SIR) algorithm or the SIR with Filtering (SIRF) algorithm [27]. The SIR algorithm is used for egg processing and the SIRF algorithm is used for slice processing. The 'AVE' images are products created using the related AVE algorithm [25] which has intermediate resolution. The pixel resolution of the slice-based SIR images is 2.225 km with an approximate effective resolution of 4km. The Egg-based SIR images have a pixel resolution of 4.45km with a effective resolution of 8-10km.

4.3 Result and Distributions

The SIR images have higher resolution than AVE images as seen in Table 1 where the egg-based SIR images are slightly better for tracking Antarctic icebergs than the egg-base AVE images. However, this result is reversed for slice based images. Slice-based AVE images are better for tracking Antarctic icebergs than slice-based SIR images, which is contrary to what was expected. This is related to the noise in the slice-based images. Along with having a higher resolution than egg-based images,

slice images are noisier. The SIR algorithm not only enhances the resolution of the image, it also enhances the noise as well. The AVE images are therefore not as noisy and are better for monitoring the spatial and temporal behavior of large Antarctic icebergs. Due to errors in the processing of the slice-based SIR images, these results may change if the analysis was repeated with new reprocessed error free slice-based images.

The horizontally polarized images are better for tracking Antarctic icebergs than vertically polarized images for all image types due to the higher contrast in σ^0 between the icebergs and the surrounding ocean. The contrast of σ^0 measurements between icebergs and sea ice is the same for both horizontally polarized images and vertically polarized images. However, the σ^0 measurements for ocean water is different between horizontal and vertical polarization measurements. Due to the structure and physical orientation of the ocean wave, vertically polarized images tend to have higher σ^0 values thereby reducing the contrast between the iceberg and it's surroundings. This reduction in contrast makes it more difficult to monitor the icebergs. Therefore horizontal polarization images are slightly better for tracking Antarctic icebergs due to the higher contrast in σ^0 measurements between the iceberg and its surroundings.

There are obstacles to tracking Antarctic icebergs using QSCAT images. The resolution of QSCAT images is limited. As noted above, the best effective resolution is 4km using slice images. Icebergs that are much smaller than 10km are not readily visible and are not tracked regularly. Limited resolution makes it difficult to distinguish the icebergs from the ice shelves when they initially break off or when they fragment. Therefore it is difficult to determine exactly when the iceberg separates from the ice shelf. Bright ice shelves have the same σ^0 values as icebergs and this sometimes creates difficulties when trying to distinguish the iceberg from the ice shelf. This is the case with icebergs B9b, C8-C10, and others in similar circumstances.

Since iceberg visibility is largely dependent on the contrast between the iceberg and its surroundings, understanding the behavior of σ^0 for icebergs and its surroundings is helpful for knowing how to track and monitor Antarctic icebergs.

The distribution of σ^0 values provides helpful information for understanding the variational patterns seen in σ^0. Several interesting observations are made when plotting the distribution of σ^0 values for both icebergs and surrounding sea ice or ocean water. Figure 4.2 shows the normalized backscatter time distribution for several icebergs for each image type. Every distribution has a bimodal characteristic. This is due to the annual Antarctic summer ice melt. Each summer the surface of the icebergs melts creating pools of surface water. This surface water reduces the σ^0 values of the icebergs thus producing a bimodal distribution of all the σ^0 values for approximately one year. Also, the mean σ^0 value for the horizontally polarized images is somewhat higher than the mean σ^0 value of the vertically polarized image. This is not only the case for iceberg σ^0 values but it is also the case for σ^0 values of sea ice or ocean water as shown in Figure 4.3. The reason for this difference is most likely due to the physical orientation of icebergs, sea ice, and ocean. Figure 4.2 and Figure 4.3 show σ^0 values tailing off to the left of each distribution and for every image type. This is caused by the Antarctic summer ice melt reducing the σ^0 values throughout the summer months.

Looking at the plots of the σ^0 values for each iceberg shows patterns in their behavior. For example Figures 4.4 and 4.5 show plots of normalized backscatter values for icebergs B14 and D11, respectively, during the year of 2000. The patterns seen with these icebergs are similar to most icebergs. During the Antarctic winter months the icebergs σ^0 values remain nearly constant. The difference between iceberg σ^0 values and the surrounding σ^0 values during these months is large enough to easily track the icebergs. The σ^0 values drop in the summer months when the temperature rises enough to cause ice surfaces to melt. When this happens the difference between iceberg σ^0 values and background σ^0 values is generally small. This creates difficulties for consistently tracking and monitoring the iceberg.

Figure 4.6 shows the distributions of the difference in normalized backscatter values between icebergs and sea ice or ocean water. The difference is almost always positive because the σ^0 values of the icebergs are generally higher than the sea ice or ocean water. In a few rare cases the icebergs may have lower σ^0 values than their

surroundings because of the summer melt. This phenomenon is seen with icebergs A38A, A38B, and occasionally the Larsen Ice Shelf. (See Figure 4.7) However, this usually only lasts for a few days because temperatures in Antarctica rarely rise above freezing.

4.4 Katabatic Winds and Icebergs

As strong katabatic winds interact with Antarctic ice shelves and large Antarctic icebergs they create Antarctic bottom water which plays a crucial role in the earth's weather system [28]. Katabatic winds are downward flowing winds. The earth's rotation draws warm air from the tropics downward to the south pole. This air is then cooled and high pressure causes this cool dense air to flow from the high continental interior down toward the coast. These winds formed on the high interior ice plateau are called inversion winds [29]. Inversion winds can turn into katabatic winds as the landscape channels and forces the airflow to converge, causing it to strengthen. Resulting katabatic winds are driven down steep slopes by gravity. In some places the land can fall 4000 feet in less than a mile. Katabatic winds can reach variable heights of 500 to 600 meters (1640 to 1970 feet) above the surface. Wind Speeds can increase from zero to 15-20 meters per second instantaneously (50 to 66 feet per second). Katabatic winds can last from a few hours to days and even weeks on end. They have also been known to reach speeds as high as 200 MPH. The winds pick up loose snow and granules of ice sweeping them across the landscape creating blizzards and transporting snow and ice hundreds of miles [30]. When these strong katabatic winds reach the frozen sea they can drive the sea ice away from the coast creating leads. As the old sea ice is pushed away from the coast new sea ice forms due to the cold katabatic winds creating cold dense water which sinks to become Antarctic bottom water. Thus we see the formation of 'pulses' coming off of the ice shelves and large icebergs, such as A43a, A43b, and A43c as seen in Figure 4.8. This same phenomenon occurs off of the edge of the Ronne and Ross ice shelves as well as many other Antarctic coastal areas. As the new sea ice forms it leaves behind most of its salt, creating cold, dense ocean water below the sea ice. This dense water called

Antarctic Bottom Water carries with it nutrients and oxygen as it flows slowly down to the ocean bottom. Seventy-five percent of all bottom water throughout the world is created in Antarctica. It is part of a larger system of global ocean currents which transports water, heat, and salt around the world. Because icebergs contribute to the creation of bottom water, the number of icebergs in Antarctic waters could become an important factor in global ocean currents. If the number of icebergs increases due to the warming of polar regions, the katabatic winds may assist in the formation of new sea ice which can create more bottom water. This may significantly affect the system of global ocean currents which impacts weather patterns and climates throughout the world. We can learn about this phenomenon by using the QSCAT images to studying the pulses, seen in Figure 4.8, over time. Thus we see that the powerful effect of the katabatic winds extends far beyond the Ronne Ice Shelf and are one of the dominant forces acting on sea ice, icebergs, and global climates.

A few icebergs cause spots of open ocean within the sea ice (See Fig 4.9). This is caused by strong winds that push the sea ice away from the iceberg. This is similar to the pulse phenomenon seen in Figure 4.8, but the areas of open ocean do not immediately freeze. Since the icebergs can extend almost 1000 feet below the surface their motion is rather slow in response to the winds and is mostly dominated by ocean currents. However, sea ice is only about 6 feet thick with the winds playing the dominant role in movement. Hence sections of open ocean are formed when winds push against the icebergs and surrounding sea ice. This same phenomenon occurs around Antarctic islands as well.

Some icebergs such as A22C, A38B, and B14 often have a ring of darker σ^0 measurements around the iceberg. This darker ring is likely to be either an artifact of the image processing or a geophysical phenomenon related to the iceberg and the surrounding sea ice.

4.5 Conclusion

Spaceborne scatterometry has become an important tool in the effort to monitor the earth's climate, forecast weather and study ocean-ice interaction. The SeaWinds scatterometer on board the QSCAT satellite provides daily σ^0 measurements across the earth's surface. With the help of BYU's SIR algorithm a set of enhanced resolution images are being produced with the data from the SeaWinds scatterometer. Due to the contrast in σ^0 measurements between icebergs and ocean or sea ice, large Antarctic icebergs are readily visible. These images are used to daily track and monitor relatively large Antarctic icebergs.

Each image type has its advantages and disadvantages. Egg-based SIR images are better for tracking icebergs than egg-based AVE images because of the improved resolution due to the SIR algorithm. However, slice-based AVE images are better for tracking icebergs than slice-based SIR images. The SIR algorithm not only enhances the resolution of the slice images, it also enhances the noise. So even though slice-based SIR images have better resolution, they are noisier than slice-based AVE images. These results could change however, due to errors found in the processing of slice-based SIR images. Slice-based AVE images provided the best results for tracking icebergs because of the images' relatively high resolution and low noise characteristics. The horizontally polarized images are better for tracking Antarctic icebergs than vertically polarized images for all image types due to the high contrast in σ^0 measurements between icebergs and surrounding ocean.

Plotting the distribution of σ^0 values for icebergs and surrounding sea ice or ocean helps in the understanding of the melt patterns for icebergs. The distribution of σ^0 values for all of the icebergs tracked shows a bimodal characteristic. This is caused by the increase in temperatures which cause the sea ice and icebergs to melt. Understanding these melt patterns is helpful for tracking icebergs during the Antarctic summers.

Strong katabatic winds interact with Antarctic ice shelves and large Antarctic icebergs to create Antarctic bottom water which plays a crucial role in the earth's weather system. If the number of icebergs increase due to the warming of the polar

regions, the katabatic winds may assist in the formation of new sea ice which can create even more bottom water than normal. This may significantly affect the system of global ocean currents which impacts weather patterns and climate throughout the world. QSCAT images may be a valuable tool for studying this phenomenon.

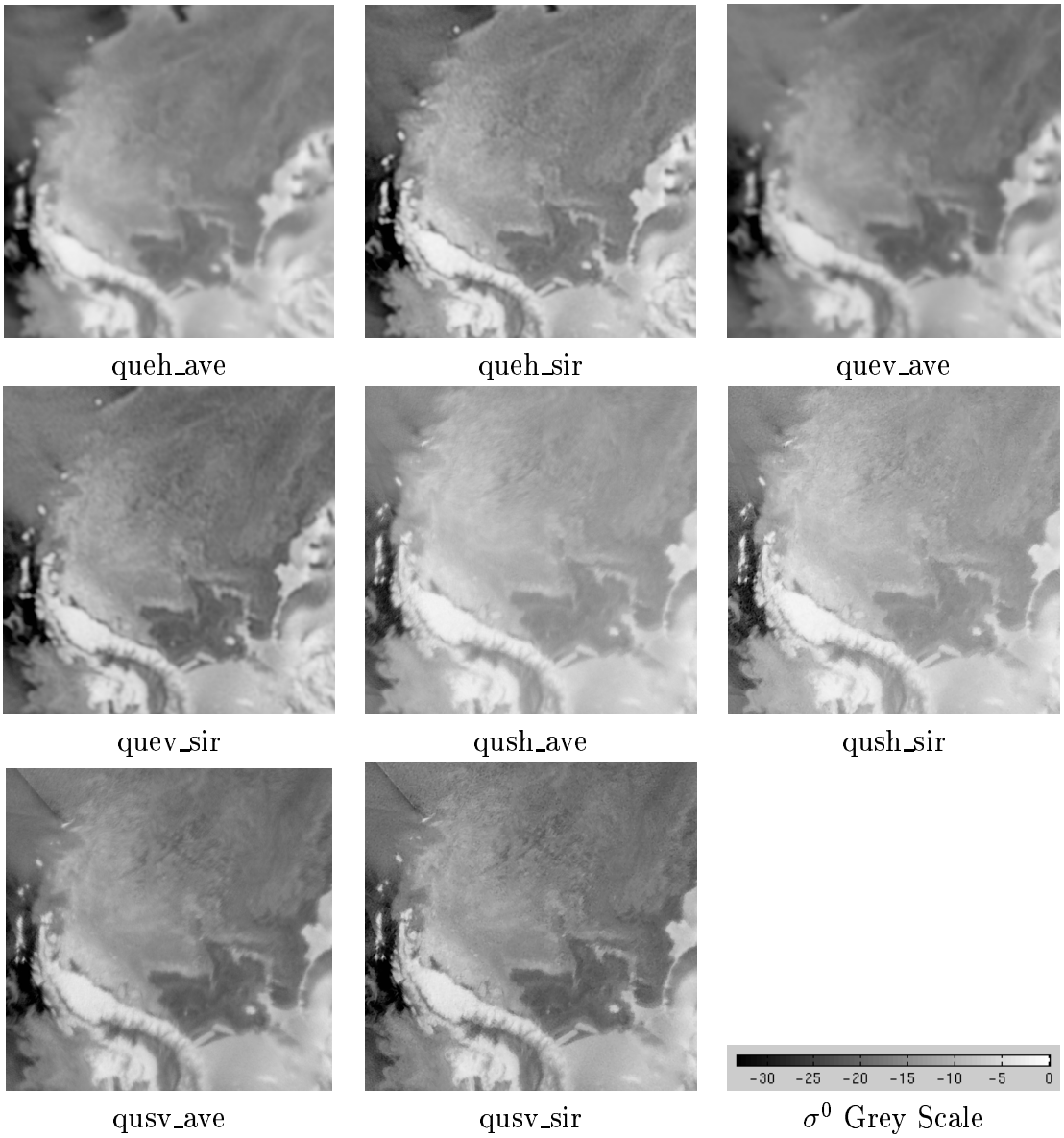

Figure 4.1: *The eight image types from the SeaWinds scatterometer (Julian Day 204)*

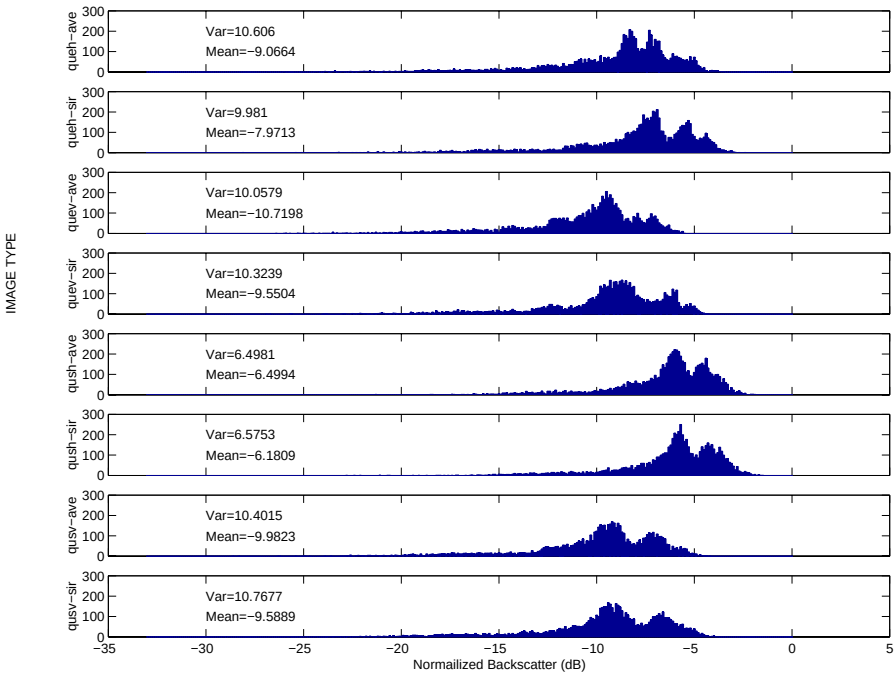

Figure 4.2: *Normalized backscatter distribution for each iceberg and for each image type.*

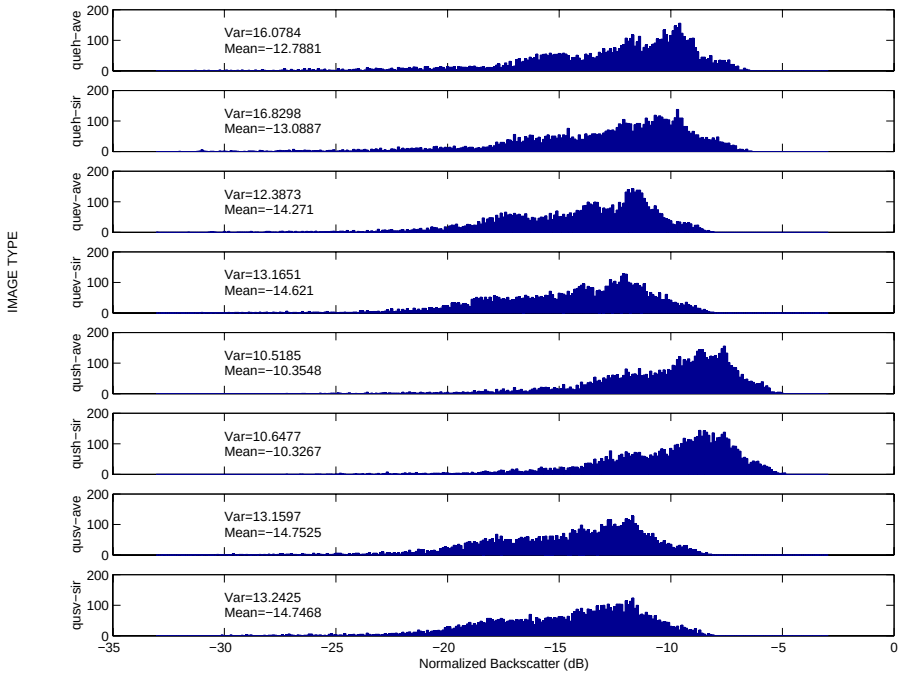

Figure 4.3: *Normalized backscatter distribution for the surrounding sea ice or ocean water.*

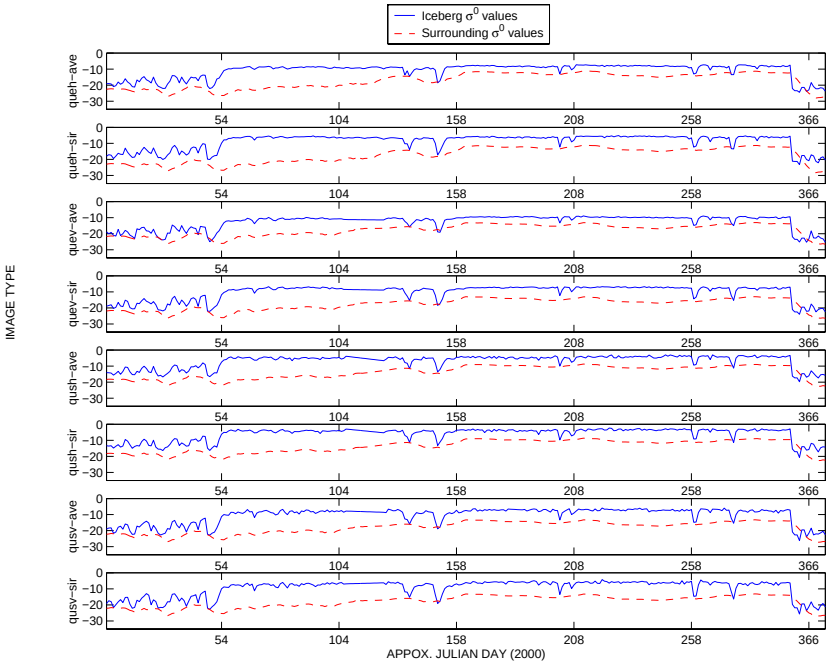

Figure 4.4: *Plot of normalized backscatter for iceberg b014 for the year of 2000.*

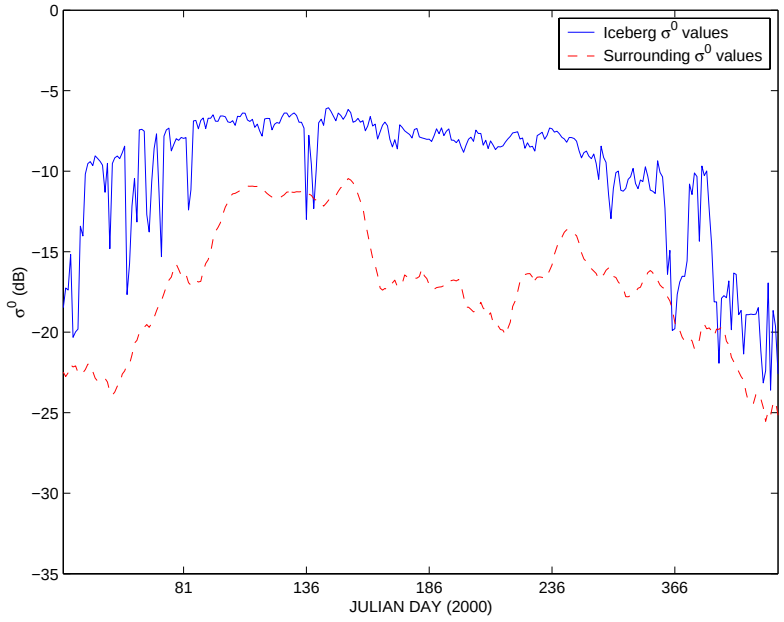

Figure 4.5: *Plot of normalized backscatter for iceberg d011 for the year of 2000.*

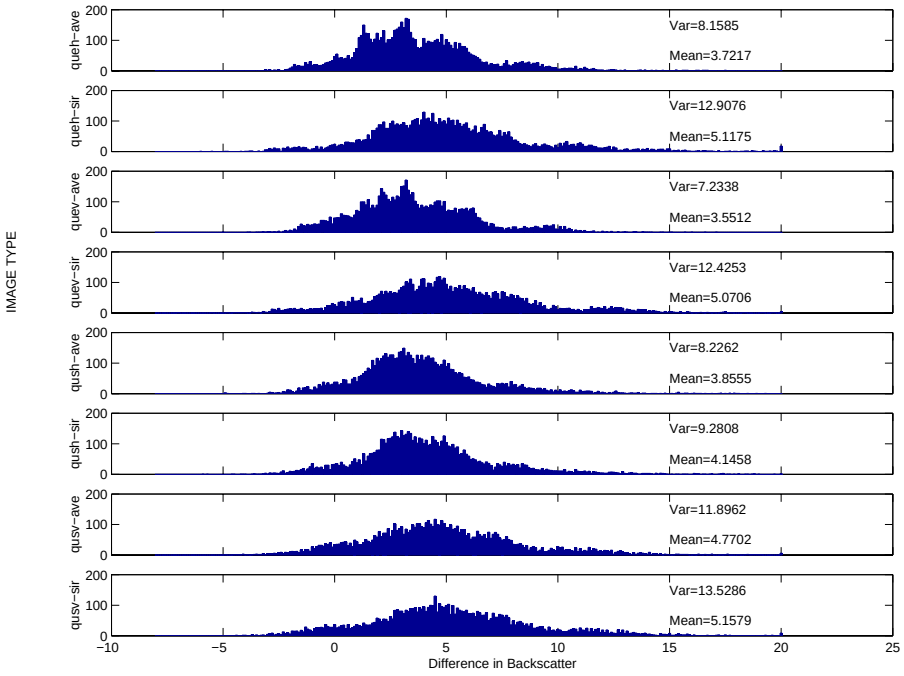

Figure 4.6: *A distribution of the difference in normalized backscatter between icebergs and sea ice or ocean water.*

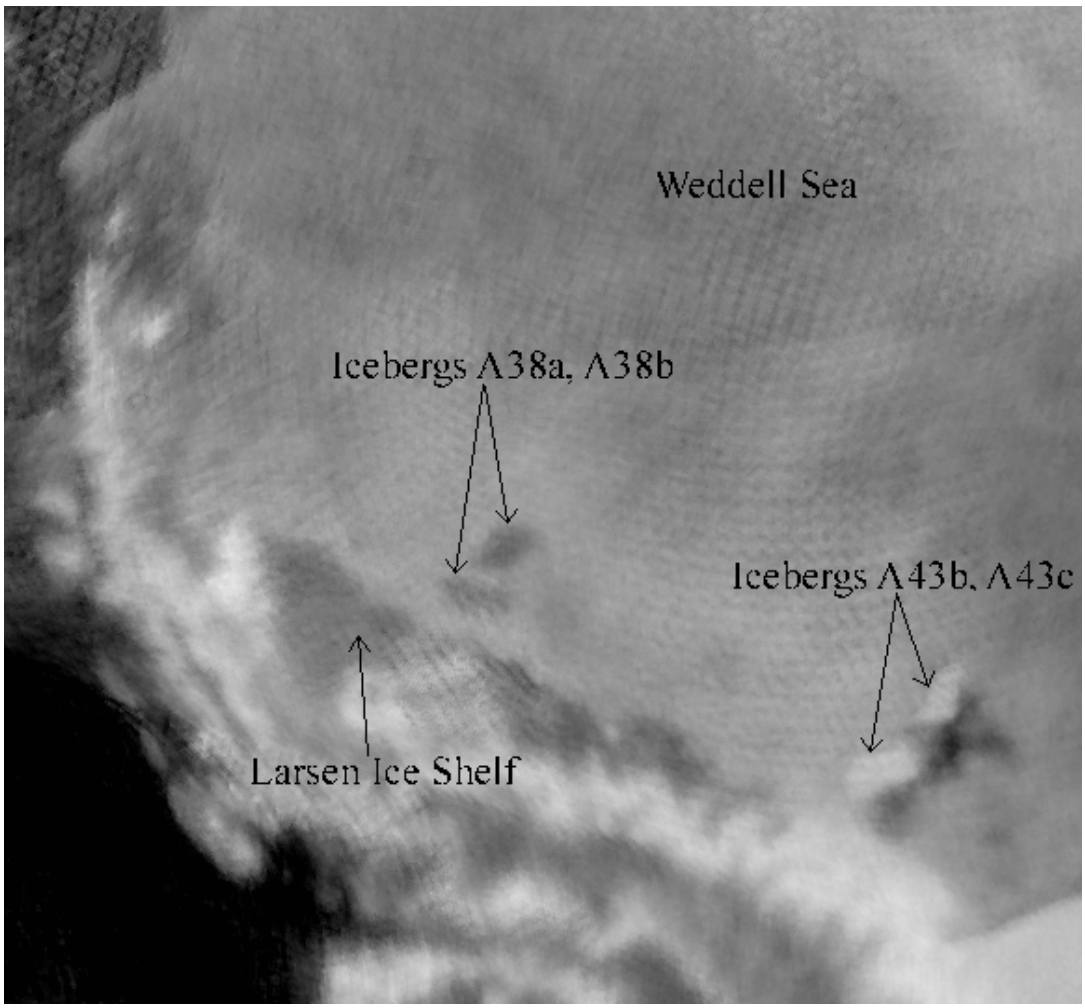

Figure 4.7: *Light and dark icebergs in the Weddell Sea (Julian Day 14, 2001). For grey scale see Figure 4.1.*

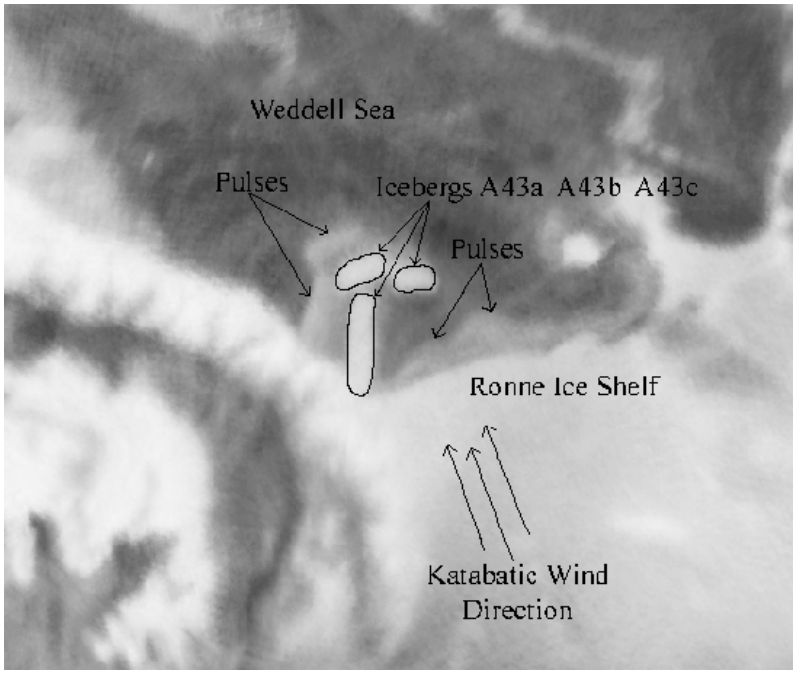

Figure 4.8: *Pulses created in the Weddell Sea. For grey scale see Figure 4.1.*

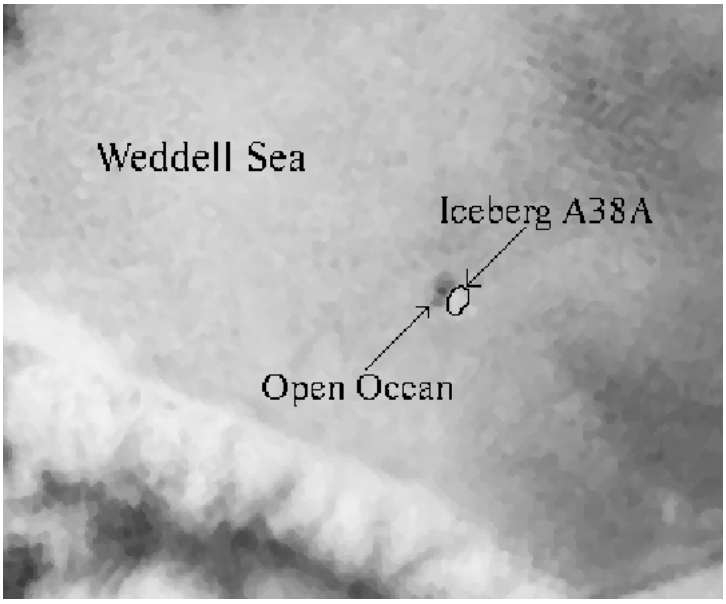

Figure 4.9: *Areas of open ocean created by winds on icebergs. For grey scale see Figure 4.1.*

Chapter 5

A Multidecadal Study of the Number of Antarctic Icebergs Using Scatterometer Data

Studying the size, frequency, and position of Antarctic icebergs helps us understand climatic changes of the Earth's frozen continent. Antarctic icebergs are regularly formed by the separation of massive sections of ice from ice shelves and glaciers. The National Ice Center (NIC) plays a major role in iceberg analysis and forecasting. The NIC uses a variety of satellite sensors to track large Antarctic icebergs and reports iceberg positions approximately every 15-20 days.

There are limitations to the NIC's iceberg tracking technique. The area covered by the images used by the NIC is limited to specific Antarctic regions due to resources required to produce and process these high resolution images. According to the NIC, the number of large Antarctic icebergs has been increasing in recent years. This increase in iceberg activity may be a result of a climatic trend, or may be an artifact of better detection techniques. A long term analysis of Antarctic iceberg activity based on scatterometer and radiometer data is presented. Our analysis suggests this increase is largely due to improved resources and technological advancements for iceberg tracking. As part of the long-term analysis, we analyze several major iceberg calving events that have taken place in recent years. These calving events may represent reasonable variability in iceberg activity. This study identifies the advantages and limitations of tracking icebergs using scatterometer data.

5.1 Introduction

Above average temperatures during the Antarctic summer months create water filled crevasses that cause ice fractures in ice shelves and glaciers. Icebergs are then formed when stress from winds and tides cause sections of ice to break from the ice shelves or glaciers. Several Antarctic ice shelves are experiencing major retreats as a result of several major calving events.

The National Ice Center (NIC) provides sea ice analysis and forecasts to meet U.S. national interests. The NIC is using a variety of satellite sensors to track and monitor Antarctic icebergs depending on their size and position. The average size of the icebergs is approximately 441 square nautical miles while some have reached as high as 3,155 square nautical miles. These large icebergs tracked at the NIC make up the vast majority of fresh water ice coming from the Antarctic continent.

Significant increases in the number of icebergs are reported by the NIC over the last 25 years. The increase is partly due to large iceberg calving events that have taken place in recent years. However, the long-term increase can be attributed to improved resources for iceberg tracking due to technological advancements. In addition, there are limitations in the NIC iceberg tracking method. Due to the high resolution of the images used by NIC, the coverage area is restricted to specific regions of the Antarctic continent. Also, due to the extensive resources needed to track icebergs, the NIC only reports an iceberg position every 15-20 days.

In order to evaluate the NIC's data and independently monitor iceberg activity, BYU utilizes scatterometer and radiometer data to track Antarctic icebergs for segments of time over the last 25 years. Data sets from five different spaceborne scatterometer and radiometer instruments are used in the study. Icebergs are tracked with each data set for various time periods from 1978 to 1999. The images provide coverage of the entire Antarctic continent and allow iceberg positions to be recorded every 1-5 days. These results are analyzed to determine the validity of the reported trend in the number of icebergs over the last 25 years. This study also identifies the advantages and disadvantages of tracking and monitoring icebergs with methods used at the NIC and methods used at BYU.

5.2 Ice Shelf Breakups

Scientific studies indicate that above-average surface temperatures over a period of a few months in the Antarctic can splinter an ice shelf and instigate a collapse [31]. Using satellite observations of melted water on the ice surface and computer simulations, scientists have demonstrated that crevasses when filled with water can crack entirely through. These crevasses are initially formed as glacial ice flows seaward. Water-filled crevasses that are 15-50 feet (5-15 meters) deep can fracture a 220 yard (200 meter) thick ice shelf. It has been theorized that the ice shelf is then held together by bridges between crevasses until a combination of winds tides, and another season of melting lead to breakup.

Mean summer temperatures play a crucial role in the creation of melt water on the ice surface. Although some areas of the Antarctic have warmed by 2.5 degrees Celsius over the last 50 years [32], few records have been kept of seasonal temperatures over the ice shelves. Data from the NIC seen in Figure 5.1 suggests that most icebergs created due to ice shelf breakups occur during the summer (JD300-JD100). This plot assumes that the first reported sightings and the birth of the iceberg occur approximately at the same time.

Many ice shelves have experienced or are expected to experience major retreats. The Larsen Ice Shelf on the Antarctic Peninsula has gone through major retreats in 1995 and 1998. Over 775 square miles (2000 square kilometers) of the northern section of this ice shelf disintegrated in 1995 during a major storm. The melt season during this retreat was over 80 days long, about 20 days longer than average. The Ross Ice Shelf in the past has generally been stable. However, within the last year the Ross Ice Shelf has experienced some major calving events. While periodic calving events are expected, some scientists theorize that excessive breaking-up of ice shelves could lead to a rise in sea level. The temporal monitoring of rather large Antarctic icebergs provides scientist with a valuable tool for determining the rate of ice shelf breakups and is important in mass balance calculations.

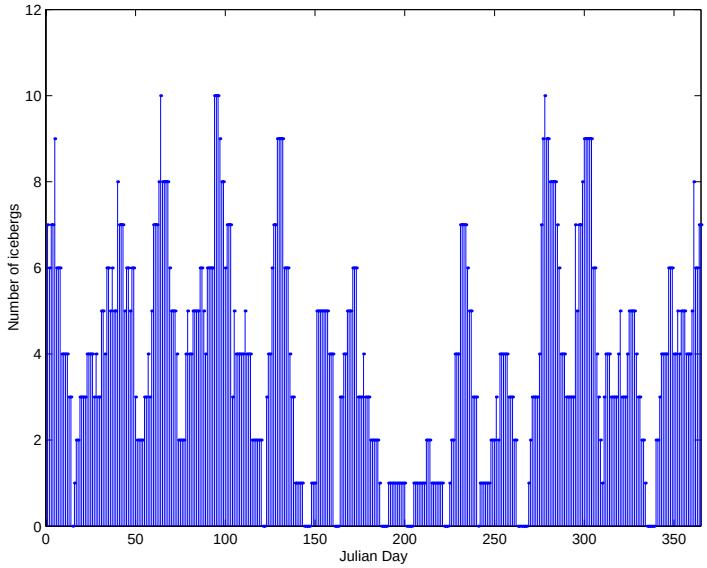

Figure 5.1: *A distribution of when icebergs were first reported by the NIC during the year.*

5.3 National Ice Center Tracks Icebergs

The National Ice Center is a multi-agency operational center representing the Department of Defense (Navy), the Department of Commerce's National Oceanic and Atmospheric Administration (NOAA), and the Department of Transportation (Coast Guard). The NIC's mission is to provide high quality sea ice analysis and forecasts designed to meet the requirements of U.S. national interests.

Antarctic icebergs must meet three basic requirements before it is tracked by the NIC. First, the iceberg must measure at least 10 nautical miles along the long axis. Second, the most recent sighting of the iceberg must have occurred within the last 30 calendar days. If it is not sighted within 30 calendar days, it is removed from the NIC's list of current icebergs. The third requirement is that the iceberg must be located below 60 degrees south latitude. There are certain exceptions to these requirements. An iceberg may be kept in the current iceberg tracking database although it has not been sighted for more than 30 days when it is grounded or locked

in sea ice. Also the NIC continues to track an iceberg until it breaks up below the resolution of satellite imagery if the iceberg's original size was 10 nautical miles or greater before its breakup.

Iceberg names given by the NIC are determined according to the Antarctic quadrant in which they were originally sighted. Quadrant A is from 0-90 degrees west longitude. Quadrant B is located between 90 degrees and 180 degrees west longitude. Quadrant C ranges from 180-90 degrees east longitude. Quadrant D is if from 90 degrees East to zero degrees east longitude. The letter of the quadrant along with a number is assigned to each iceberg tracked. For example, iceberg B4 is the fourth iceberg identified in quadrant B. If this iceberg breaks up into separate icebergs they are named B4A, B4B, and B4C etc.

A distribution of the sizes of the Antarctic icebergs reported by the NIC since 1976 is shown in Figure 5.2. Most of the icebergs tracked by the NIC range in size from 50 to 600 square nautical miles. The average size of the icebergs tracked by the NIC is just over 441 square nautical miles. The largest iceberg ever reported was iceberg B15 which was 3,155 square nautical miles and was first reported in March of 2000. It is assumed that due to their tremendous size, icebergs make up the majority of the glacial ice coming from the Antarctic continent.

The NIC uses a variety of methods for tracking and monitoring Antarctic icebergs. The most commonly used instrument is the Defense Meteorological Satellite Program (DMSP) F13 satellite. The DMSP F13 satellite is in a near circular, sun synchronous, polar orbit. This satellite provides global visible and infrared images of the earth with its Operational Linescan System (OLS). Figure 5.3a shows an image of the iceberg B10A through clouds using DMSP OLS infrared imagery from F13 on Julian day 238, 1999. The satellite measures data at a 0.56 km resolution, which is averaged on board the satellite to produce global coverage at 2.7 km resolution. A key limitation to using the DMSP instrument is the obstruction in visibility due to the local cloud cover. Due to this limitation, iceberg B10A was lost to the NIC and later located using scatterometer images produced by BYU. The OLS images offer high resolution but low coverage due to a small swath and image processing.

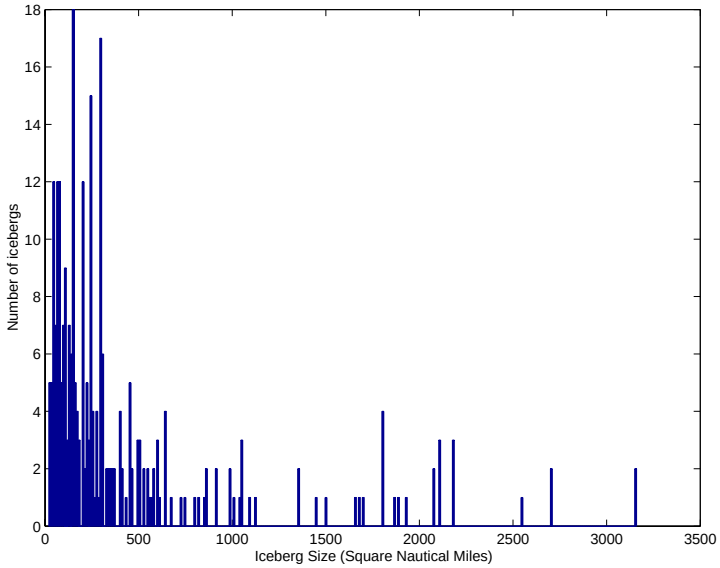

Figure 5.2: *Distribution of the sizes of the Antarctic icebergs as reported by the NIC.*

The Advanced Very High Resolution Radiometer (AVHRR), mounted on board NOAA meteorological satellites is also used by the NIC to track Antarctic icebergs. The AVHRR operates in the visible, infrared, and thermal spectrum with a resolution of 1.1 km. Figure 5.3c shows an AVHRR image of icebergs B10A and A22B. The advantages and limitations of using AVHRR images to track Antarctic icebergs are similar to the advantages and limitations of the DMSP OLS. These images have a relatively high resolution but local cloud cover obscures the visibility of the icebergs.

The NIC also currently obtains iceberg positions provided by the MERS lab at BYU. The BYU MERS lab uses enhanced resolution images obtained from the SeaWinds scatterometer on board the satellite QSCAT. The MERS lab's method for tracking Antarctic icebergs is discussed in Section 3.2.

The NIC also infrequently tracks icebergs with SAR images from the RADARSAT instrument on board the Earth Observation (EO) satellite and ship-reported iceberg positions. A RADARSAT wide scan SAR B image of icebergs in the Weddell Sea is shown in Fig 5.3b. RADARSAT images are not restricted by the presence of clouds,

fog, smoke, or darkness. These images have a very high resolution (from 8 to 100 meters) but limited coverage.

The time between reported iceberg positions for the NIC typically varies from 15 to 20 days. One reason for the long interval is due to the tremendous effort it takes to obtain images and locate icebergs. Another reason is because the relatively slow movement of many of the icebergs may not necessitate daily iceberg tracking by the NIC.

Figure 5.4 shows the number of icebergs tracked by the NIC from 1976 to 2001. This figure also shows the number of icebergs tracked by the BYU MERS lab for different time periods. The icebergs tracked by the NIC in the late 1970's are sporadic and few, most likely due to the NIC's limited resources during this time period. During the early 1980's the number of icebergs tracked remains relatively constant (from 4 to 6).

During 1986-1987, the number of icebergs tracked by the NIC significantly increases to between 10-15. There may be several reasons for this sudden increase. The increase could be due to large sections of Antarctic ice shelves breaking off of the main ice shelf. Another reason may be the technological advancement involving more advanced computers and improved satellite instruments which provides better resources for tracking the icebergs. There also may have been an increase in the NIC's effort to track a larger number of icebergs during this time.

Between 1987-1996 the number of icebergs fluctuate and then there are significant jumps during late 1996, early 1999, and early 2000. The fluctuations appear to be reasonable variations.

The majority of the Antarctic icebergs calve from the Ronne Ice Shelf, the Filchner Ice Shelf, the Larsen Ice Shelf, and the Ross Ice Shelf. As shown in Figure 5.5, the largest cluster of icebergs reported by the NIC have come from the Weddell Sea. These icebergs calved from either the Ronne Ice Shelf, Filchner Ice Shelf, or the Larsen Ice Shelf and then travel north between 20 degrees to 50 degrees west longitude along what has been named 'Iceberg Alley'. The second largest group of icebergs is located in the Ross Sea. These icebergs calve from the Ross Ice Shelf and travel west

along the Antarctic coast being carried by an Antarctic coastal current. Many of these icebergs eventually reach the Weddell Sea and then travel north through the 'Iceberg Alley'. A few icebergs traveling west with the Antarctic coastal current turn north near 90 degrees east longitude, getting caught in the Antarctic Circumpolar Current (ACC) and travel northeast. Other icebergs in the Ross Sea travel north until they are caught in the ACC and then they move east through the Drake Passage, ending up in 'Iceberg Alley'.

Most of the recent icebergs in the Ross Sea were first reported in 2000 due to several large calving events. Before this time, very few icebergs had been reported breaking from the Ross Ice Shelf.

5.4 Tracking Icebergs at BYU

As shown in Figure 5.4, the number of icebergs reported by the NIC has gradually been increasing for the last 25 years. In order to evaluate the NIC's data and independently monitor iceberg activity, BYU utilizes scatterometer and radiometer data to track Antarctic icebergs for various segments of time over the last 25 years.

Data sets from five different spaceborne scatterometer and radiometer instruments are used in the study. For each data set resolution enhancement is performed by BYU's Scatterometer Image Reconstruction (SIR) and SIR Filtering (SIRF) algorithms. The SIRF algorithm provides enhanced-resolution scatterometer and radiometer images by combining data from multiple overlapping passes of the satellite.

The scatterometer instruments used in this study are the Seasat-A Satellite Scatterometer (SASS), the European Space Agency's Remote Sensing Satellite 1(2) (ERS1(2)), the NASA Scatterometer (NSCAT), and the QuikSCAT/SeaWinds scatterometer (QSCAT). In addition to the use of scatterometers, the Special Sensor Microwave/Imager (SSM/I), a microwave radiometer, is utilized. Table 5.1 provides information on the number of days of data used per image, the polarization used, the resolution in kilometers per pixel, and the frequency band used for each instrument. Although these images are "enhanced resolution", varying from 8-25 km, they still have a much lower resolution than many of the other instruments used by the NIC.

Table 5.1: *Information for sensors used to track Antarctic icebergs.*

Sensor	Days/image	polarization	km/pix	Freq
SASS	23	h-pol	4.45	Ku-Band
ERS2	5	v-pol	8.9	C-Band
NSCAT	5	h-pol	4.45	Ku-Band
SSM/I	1	h-pol	8.9	19.35 GHz
QSCAT(egg)	1	h-pol	4.45	Ku-Band

With resolution-enhanced images, distinct features of the Antarctic continent can be seen. Figure 5.6 and 5.7 show enhanced-resolution images of the Antarctic continent and the Weddell Sea from the five different sensors mentioned. Sea ice, ice shelves, and land features can be clearly distinguished as measurement values vary across the Earth's surface. Large Antarctic icebergs are identified as objects of contrasting measurement values against the surrounding ocean or sea ice. Although each instrument provides a slightly different resolution, icebergs are clearly visible in all images. Figure 5.8 shows images of different icebergs from QSCAT and ERS1.

Icebergs are tracked with each data set for various time periods from 1976 to 1999. Animated movies are created for each time period monitored. These movies are used to manually identify and track icebergs found in the Antarctic region. An iceberg is first identified if it is clearly distinguishable from land or ice shelves and if it passes either of two criteria. First, icebergs are identified if they are located in the same positions as indicated by the NIC. Second, icebergs are identified when they were not indicated by the NIC but the iceberg is clearly distinguishable and motion is detected. A few icebergs are additionally identified where they were not reported by the NIC and motion was not detected. In these cases the icebergs were clearly not a part of any land feature or ice shelf. The icebergs tracked at BYU versus icebergs reported by the NIC are shown in Table 5.2 and Table 5.3.

Although motion plays a critical role in identifying icebergs, some icebergs are identified when there is no detectable motion during some or all of the tracking period.

Table 5.2: *Icebergs Tracked at BYU vs. Icebergs Reported by the NIC.*

1978 JD188-281		1992 JD001-365		1994 JD022-365		1996 JD001-126		1996 JD259-365	
NIC	SASS	NIC	ERS1	NIC	ERS1	NIC	ERS1	NIC	ERS2
A1	SA1=A1	A22	E1=A22	A27		A27		A27	
A2	SA2=A2	A28	E2=A28	A33		A22A	E1=A22A	A34	
	SA3	A29	E3=A29	A22A	E1=A22A	A22B	E2=A22B	A35	E1=A35
	SA4	A31	E4=A31	A22B	E2=A22B	A23A	E3=A23A	A22A	E2=A22A
	SA5	A23A	E5=A23A	A23A	E3=A23A	A23B	E4=A23B	A22B	E3=A22B
	SA6	A23B	E6=A23B	A23B	E4=A23B	B9A	E5=B9A	A23A	E4=A23A
	SA7	A24A		B10	E5=B10	B9B	E6=B9B	A23B	E5=A23B
	SA8=B1	A24B		B9A	E6=B9A	B10A	E7=B10A	B9A	E6=B9A
	SA9=C2	A24C		B9B	E7=B9B	B10B	E8=B10B	B9B	E7=B9B
	SA10	A24D		C5	E8=C5	C8	E9=C8	B10A	E8=B10A
	SA11=D2	B10	E7=B10		E9=C10	C9		B10B	E9=B10B
	SA12=D3	B7B	E8=B7B		E10	D10		C8	E10=C8
	SA13	B9A	E9=B9A		E11		E10=C10	C9	
		B9B	E10=B9B				E11=D11	C10	E11=C10
		C5					E12	D11	E12=D11
		C6	E11=C6						E13=D10
		C7	E12=C7						E14
			E13=C10						E15
			E14						
			E15						
			E16						
			E17						
			E18						
			E19						
Total: 2	13	17	19	10	11	12	12	15	15

Table 5.4 lists icebergs tracked at BYU from 1978-1999 which had no discernable movement at some point during the observation period. None of the icebergs displayed any motion during their initial tracking period, suggesting that they were grounded before being tracked by BYU. About two-thirds of the icebergs shown in the Table 5.4 never displayed any discernable movement during the entire tracking period. A third of the icebergs showed no movement during the first few tracking periods and then eventually showed some movement during the last tracking periods. From Table 5.4, we see that icebergs showing no movement (grounded) make up a large percentage of the total number of icebergs.

5.4.1 The BYU Iceberg Database

Using five different satellite instruments, we have produced one of the longest and most detailed Antarctic iceberg databases. The BYU database includes icebergs identified during 1978 and icebergs from 1992 to the present. Many icebergs not tracked by the NIC are included in this database. For example, the NIC recorded

Table 5.3: *Icebergs Tracked at BYU vs. Icebergs Reported by the NIC.*

1996 JD259-365		1998 JD001-365		1999 JD200-365		1999 JD190-352		1999 JD202-365	
NIC	NSCAT	NIC	ERS2	NIC	ERS2	NIC	SSM/I	NIC	QSCAT
A27	N1=A27	A027		A27		A27		A27	Q1=A27
A34		A36	E1=A36	A39		A39		A39	Q2=A39
A35	N2=A35	A37		A41		A41		A41	
A22A	N3=A22A	A39	E2=A39	A22A	E1=A22A	A22A	S1=A22A	A22A	Q3=A22A
A22B	N4=A22B	A22A	E3=A22A	A22B	E2=A22B	A22B	S2=A22B	A22B	Q4=A22B
A23A	N5=A23A	A22B	E4=A22B	A22C	E3=A22C	A22C	S3=A22C	A22C	Q5=A22C
A23B	N6=A23B	A22C	E5=A22C	A23A	E4=A23A	A23A	S4=A23A	A23A	Q6=A23A
B9A	N7=B9A	A23A	E6=A23A	A35A	E5=A35A	A35A	S5=A35A	A35A	Q7=A35A
B9B	N8=B9B	A23B	E7=A23B	A35B	E6=A35B	A35B		A35B	Q8=A35B
B10A	N9=B10A	A35A	E8=A35A	A35C		A35C		A35C	Q9=A35C
B10B	N10=B10B	A35B		A38A	E7=A38A	A38A	S6=A38A	A38A	Q10=A38A
C8	N11=C8	A35C		A38B	E8=A38B	A38B	S7=A38B	A38B	Q11=A38B
C9	N12=C9	A38A	E9=A38A	A38D		A38D		A38D	
C10	N13=C10	A38B	E10=A38B	A40A		A40A		A40A	Q12=A40A
D11	N14=D11	A38C		B9A	E9=B9A	B9A	S8=B9A	B9A	Q13=B9A
	N15=D10	B9A	E11=B9A	B9B	E10=B9B	B9B	S9=B9B	B9B	Q14=B9B
	N16=D14	B9B	E12=B9B	B10A	E11=B10A	B10A	S10=B10A	B10A	Q15=B10A
	N17	B10A	E13=B10A	C8	E12=C8	C8	S11=C8	C8	Q16=C8
	N18	C8	E14=C8	C9		C9		C9	Q17=C9
	N19	C9		C10	E13=C10	C10	S12=C10	C10	Q18=C10
		C10	E15=C10	C11		C11		C11	Q19=C11
		C11	E16=C11	C12	E14=C12	C12		C12	Q20=C12
		C12		D11	E15=D11	D11	S13=D11	D11	Q21=D11
		D11	E17=D11		E16=A23B		S14		Q22=A23B
		D12	E18=D12		E17=D15		S15		Q23=D14
		D14			E18				Q24=D15
		D15	E19=D15		E19				Q25=B14
			E20		E20				
			E21		E21				
			E22		E22				
			E23		E23				
Total:15	19	27	23	23	23	23	15	23	25

only two icebergs in the Antarctic region in 1978 while BYU tracked 13 icebergs during this time.

There are several advantages to BYU's iceberg database. First, iceberg positions are reported every 1 to 5 days in BYU's iceberg database versus every 15 to 20 days in the NIC's database. Figure 5.10 shows the detailed path for two icebergs tracked by BYU. This figure displays the complicated motion through the oceans around Antarctica not evidenced in the NIC data. A comparison of reported iceberg position by the NIC and BYU can be seen in Figures 5.5 and 5.9 respectively. The higher temporal resolution provides information about the ocean currents that are primarily responsible for the iceberg's motion. It also gives more accurate and timely position measurements for mariners operating in the Antarctic regions. The second major advantage to BYU's iceberg database is the ability to extend the tracking of

Table 5.4: *Icebergs tracked from 1978-1999 that had no discernable movement at some point during the observation period.*

NIC ID	1978 JD188-281	1992 (Ea) JD001-365	1994 (Eb) JD022-365	1996 (Ec) JD001-126	1996 JD259-365	1998 JD001-365	1999 JD190-352	1999 JD202-365
	SASS	ERS	ERS	ERS	NSCAT	ERS2	SSM/I	QSCAT
A23A	-	X	X	X	X	X	X	X
A22	-	X						
A22A	-	-	X	M	M	M	M	M
B9A	-	X	X	X	X	M	M	M
B9B	-	X	X	X	X	X	X	X
C2	X							
C5	-	X	M					
C8	-	-	-	X	X	X	X	X
C9	-	-	-	X	X	X	X	M
C10	-	X	X	X	X	X	X	X
C11	-	-	-	-	-	X	X	X
C12	-	-	-	-	-	X	X	X
D3	X							
D11	-	-	-	X	M	M	M	M
D14	-	-	-	-	X	X	X	X
D15	-	-	-	-	-	X	X	X
SA10	X							
Ea18	-	X						

X = No Movement Detected, M = Some Movement Detected

several icebergs beyond the NIC's range. For example, iceberg A35 was first reported by the NIC on Julian Day (JD) 347 in 1996 at latitude 75.4 South and longitude 29.6 West. However, A35's original position was reported by BYU on JD136 in 1994 at latitude 65.73 south and longitude 87.06 east. Iceberg A35 originated from the same iceberg as D11 and D12. Given this evidence icebergs A35, D11, and D12 should have been named D11A, D11B, and D11C. As another example, iceberg B14 was first tracked by the NIC on JD005 in 2000 at latitude 67.1 south and longitude 178 west. With the help of ERS images, this same iceberg was tracked at BYU on JD265 in 1997 at latitude 74.11 south and longitude 130.21 west.

5.4.2 Number of Icebergs Tracked At BYU versus the NIC

There are distinct differences in the number of icebergs tracked at BYU versus the NIC. Figures 5.11 and 5.12 and Tables 5.2 and 5.3 show the icebergs tracked by BYU versus those tracked by the NIC. During 1992 the NIC tracked 17 icebergs

while BYU tracked 19 icebergs. Many of the 1992 icebergs tracked by BYU are the same icebergs tracked by the NIC. Yet, seven icebergs are identified at BYU which are not identified by the NIC. Also, five icebergs identified by the NIC were not identified by BYU, probably due to their small size. Each tracking period exhibits the same trend. The differences in the number of icebergs tracked are related to the advantages and limitations of the methods used. As addressed earlier, the NIC uses images with very high resolution. This allows them to track smaller icebergs than can't be tracked using the limited resolution scatterometer and radiometer images. Most of the icebergs detected by the NIC and not by BYU are of relatively small size. The disadvantage to using the NIC's high resolution images is the relatively low coverage area. Because of the low coverage the NIC generally only tracks icebergs in specific Antarctic regions. The scatterometer and radiometer images produced at BYU have a lower resolution but have a broad coverage area. Images by SSM/I and QSCAT provide daily coverage of the entire Antarctic continent and surrounding oceans. Broad coverage allows new icebergs to be located and monitored over a wider coverage area and with frequent (daily) coverage.

Another reason for the difference in the number of icebergs tracked between the NIC and BYU is related to the different types of images used. Figure 5.12 shows a comparison of the number of icebergs tracked by the NIC versus icebergs tracked by BYU using various radar instruments during 1996 and 1999. The number of icebergs monitored by the NIC and those tracked using the ERS images are very similar for both years as well as for most tracking periods. There are more icebergs observed using NSCAT and QSCAT images than any other method because of the improved resolution of NSCAT and QSCAT over the ERS and SSM/I images and the broad coverage area for both NSCAT and QSCAT images. SSM/I images were not as useful and fewer icebergs were visible than other sensors used. Figure 5.11 shows a comparison for the number of icebergs tracked with different methods and for different tracking time periods.

Are the numbers of Antarctic icebergs increasing? Figure 5.4 shows the number of icebergs tracked over time by the NIC and at BYU. This plot shows the number

of icebergs increasing for both the NIC and for BYU. It is interesting to note the difference in tracking numbers for BYU and the NIC. In 1978 the NIC tracked two icebergs while 13 icebergs were tracked by BYU. This difference may be due to the limited amount of resources available to the NIC at the time. During 1992, there is also a significant difference in the number of icebergs tracked. This may be due to the improved coverage capabilities of the sensors used at BYU versus the NIC. Since 1995 the number of icebergs tracked for both the NIC and BYU are very similar. This is due largely to BYU occasionally supplying iceberg tracking information to the NIC. The main increase in the number of icebergs from 1999 to 2001 is largely due to several large calving events from the Ronne and Ross Ice Shelves. Also, a greater number of icebergs are identified due to the improved resolution of images used and due to improved tracking techniques. Based on BYU's tracking the number of icebergs did not change significantly from 1978-1999. The number of icebergs being tracked has been increasing since 1999. However, the data is insufficient to determine whether this is a cyclic event or a long term increase. As technology improves, smaller icebergs will be included in the list of icebergs tracked.

5.5 Conclusion

The NIC plays a major role in sea ice analysis and forecasts. As a part of its mission the NIC is using a variety of satellite sensors to track many large Antarctic icebergs. The NIC now obtains many of its iceberg positions from BYU due to BYU's efforts in recent years to track icebergs.

The number of icebergs tracked by the NIC has risen over the last 25 years. This increase is largely due to major iceberg calving events that have taken place in recent years. It is also due to improved resources for iceberg tracking and to technological advancements. However, there are limitations in the NIC's iceberg tracking techniques. The area covered by the image used by the NIC are limited to specific areas of the Antarctic continent. This limitation of low coverage is due to the large amount of resources required to produce these high resolution images. Because of the extensive amount of resources required to track icebergs the NIC reports iceberg positions every 15-20 days.

To evaluate the NIC's results and monitor iceberg activity, BYU is utilizing scatterometer and radiometer data to track Antarctic icebergs for different segments of time over the last 25 years. Five data sets from various instruments were chosen to be used in the study. Icebergs were tracked independently with each data set for time periods between 1976 to 2001. Each image used provided coverage of the entire Antarctic continent allowing frequent positions to be reported for each iceberg. We report an increasing trend in the number of visible icebergs over the last 20-25 years. However, this trend is only significant from 1999 to 2001 due to several major calving events during these years. From 1978-1998 the number of icebergs remains fairly constant although there is a significant data gap from 1978 to 1992. Whether this recent increasing trend represents a natural variability in the number of icebergs or a long term increase is unknown. More data is needed.

This study has shown the advantages and limitations of tracking icebergs with methods used by the NIC versus methods used at BYU. Our increased ability to observe and track the formation of large Antarctic icebergs using remote satellite sensors has contributed significantly to our awareness in icebergs formed in Antarctica.

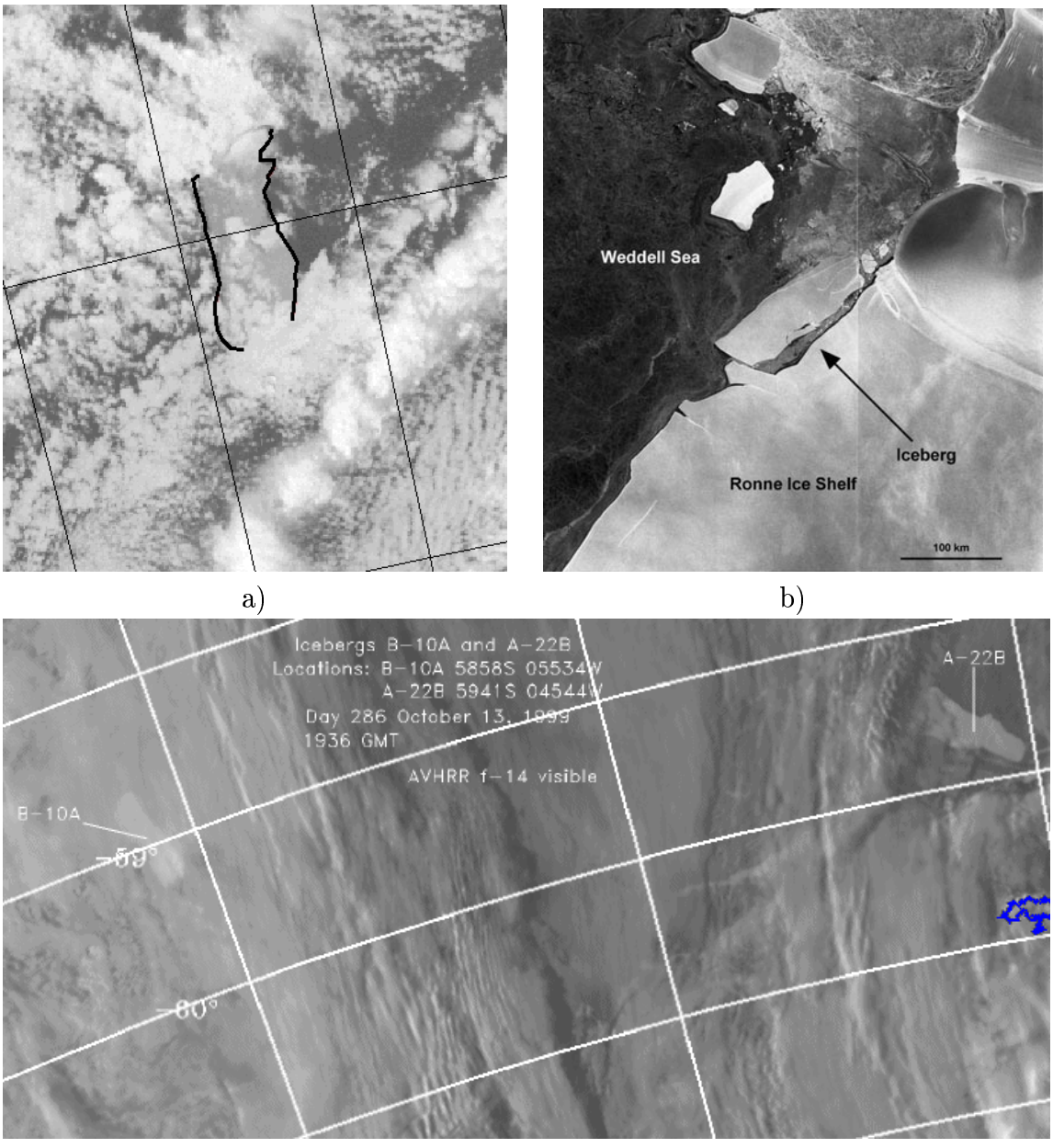

Figure 5.3: *Iceberg images: a) Outline of B10A through clouds using DMSP OLS infrared imagery from F13 (Julian Day 238, 1999). b) RADARSAT Wide ScanSAR B image of icebergs in the Weddell Sea, acquired on October 20, 1998. c) AVHRR image of B10A and A22B (Julian Day 286, 1999).*

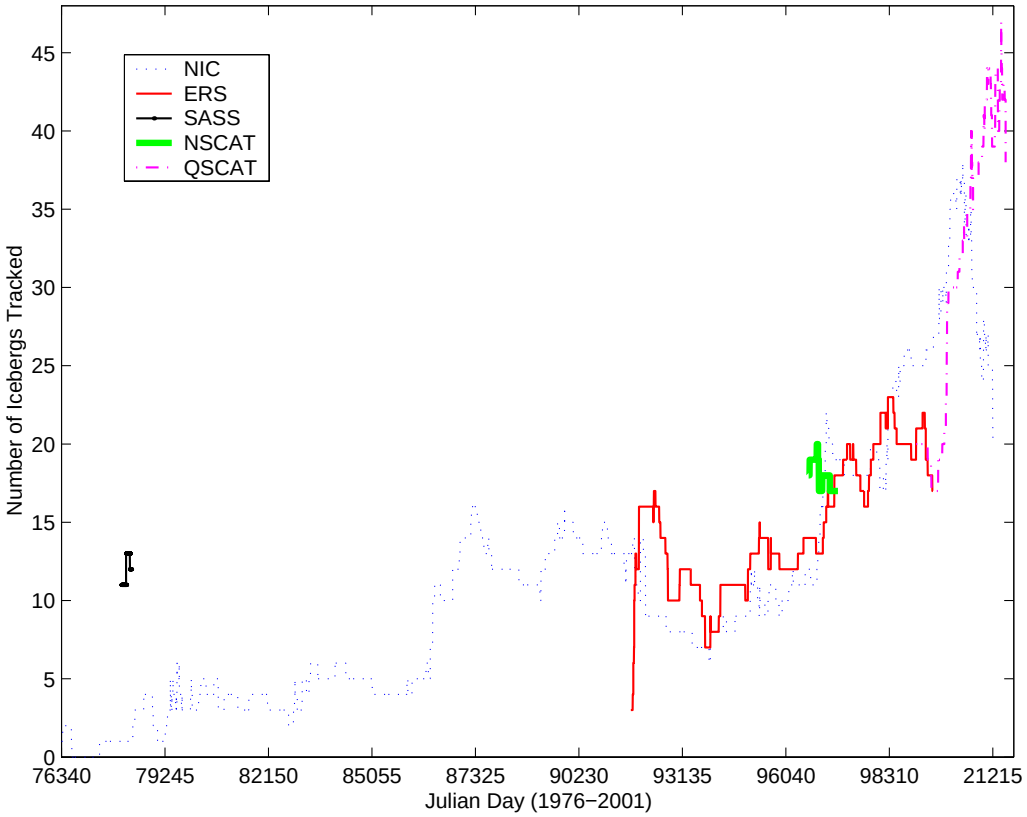

Figure 5.4: *Number of icebergs tracked over time.*

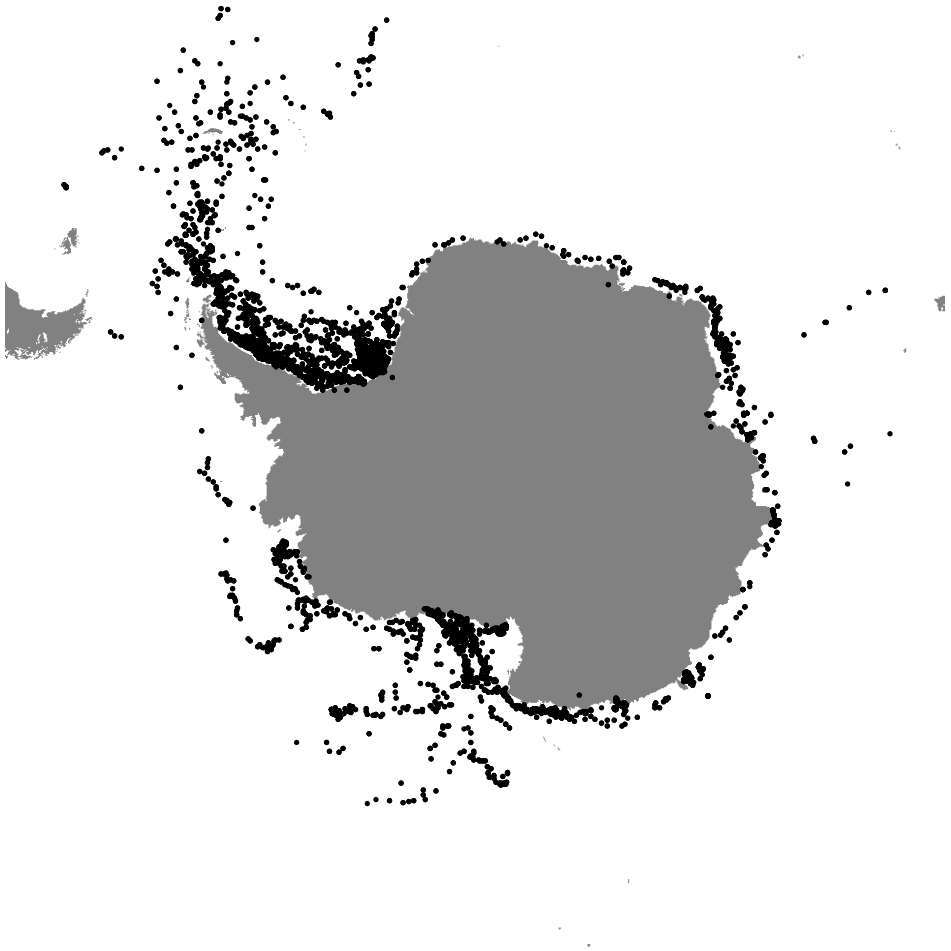

Figure 5.5: *All positions reported for all icebergs tracked by the NIC (1978-2001), shown as black dots.*

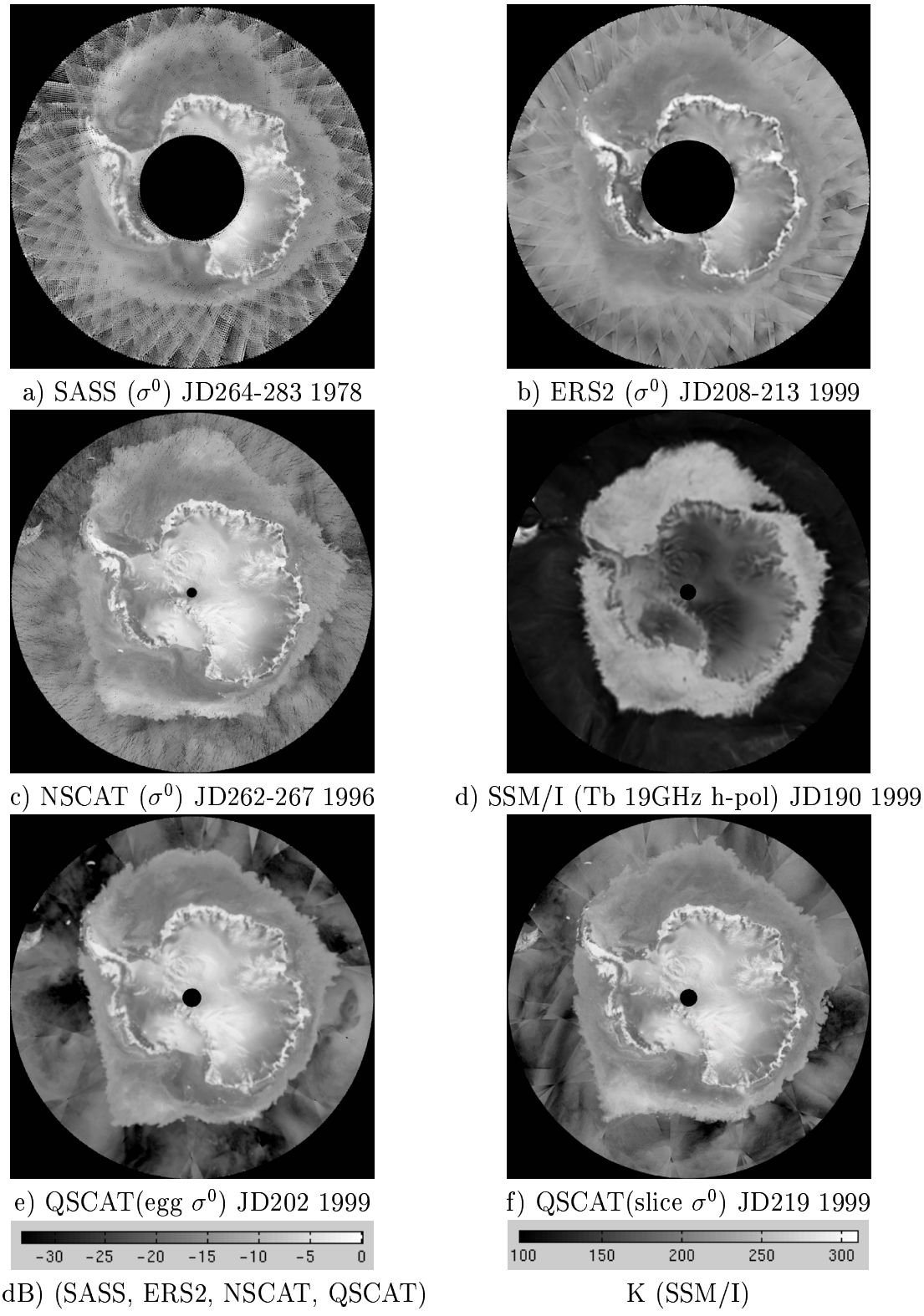

Figure 5.6: *Enhanced resolution images of Antarctica for various sensors (See Table 5.1 for details).*

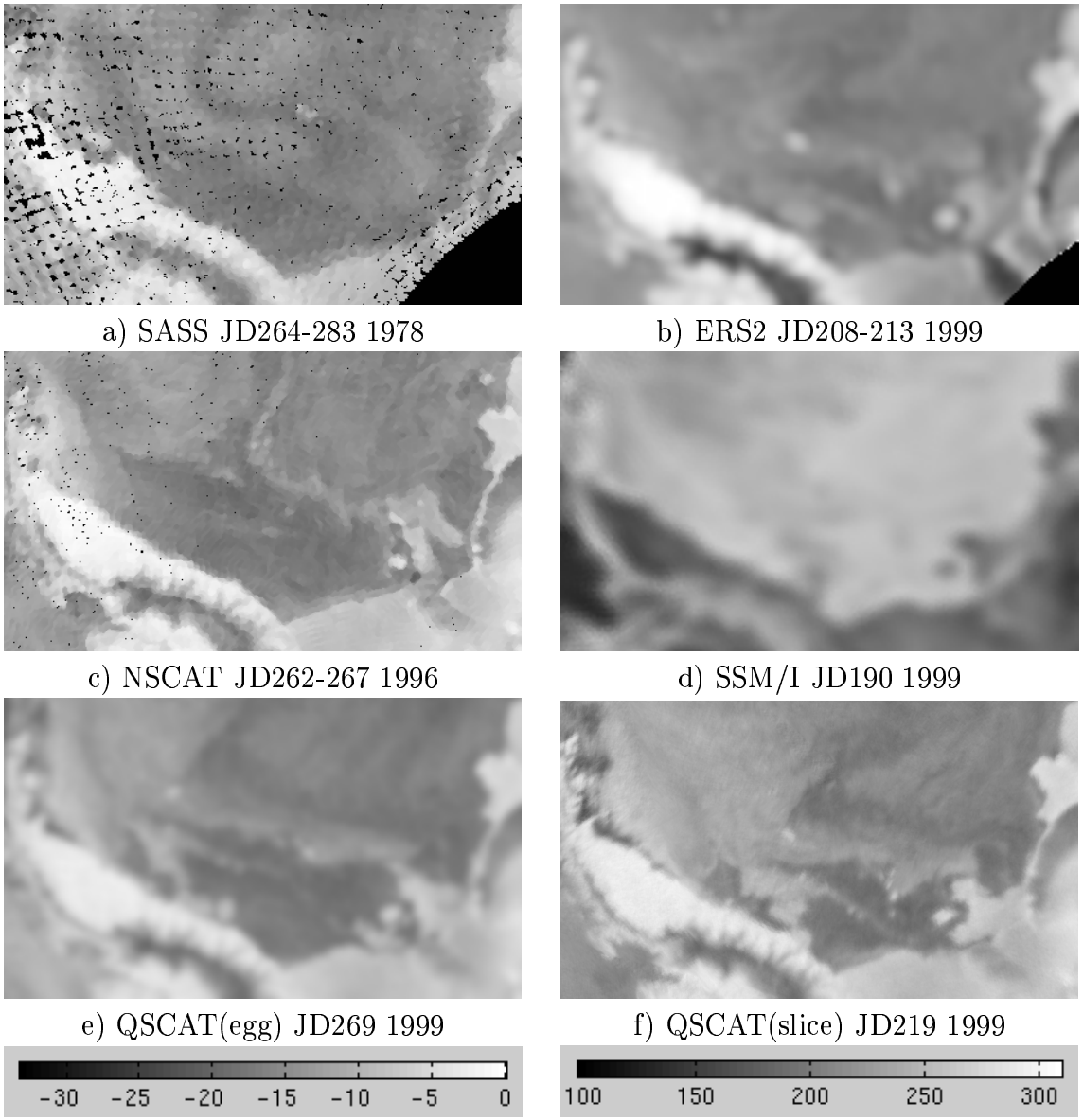

Figure 5.7: *Enhanced resolution images of the Weddell Sea for various sensors (See Table 5.1 for details).*

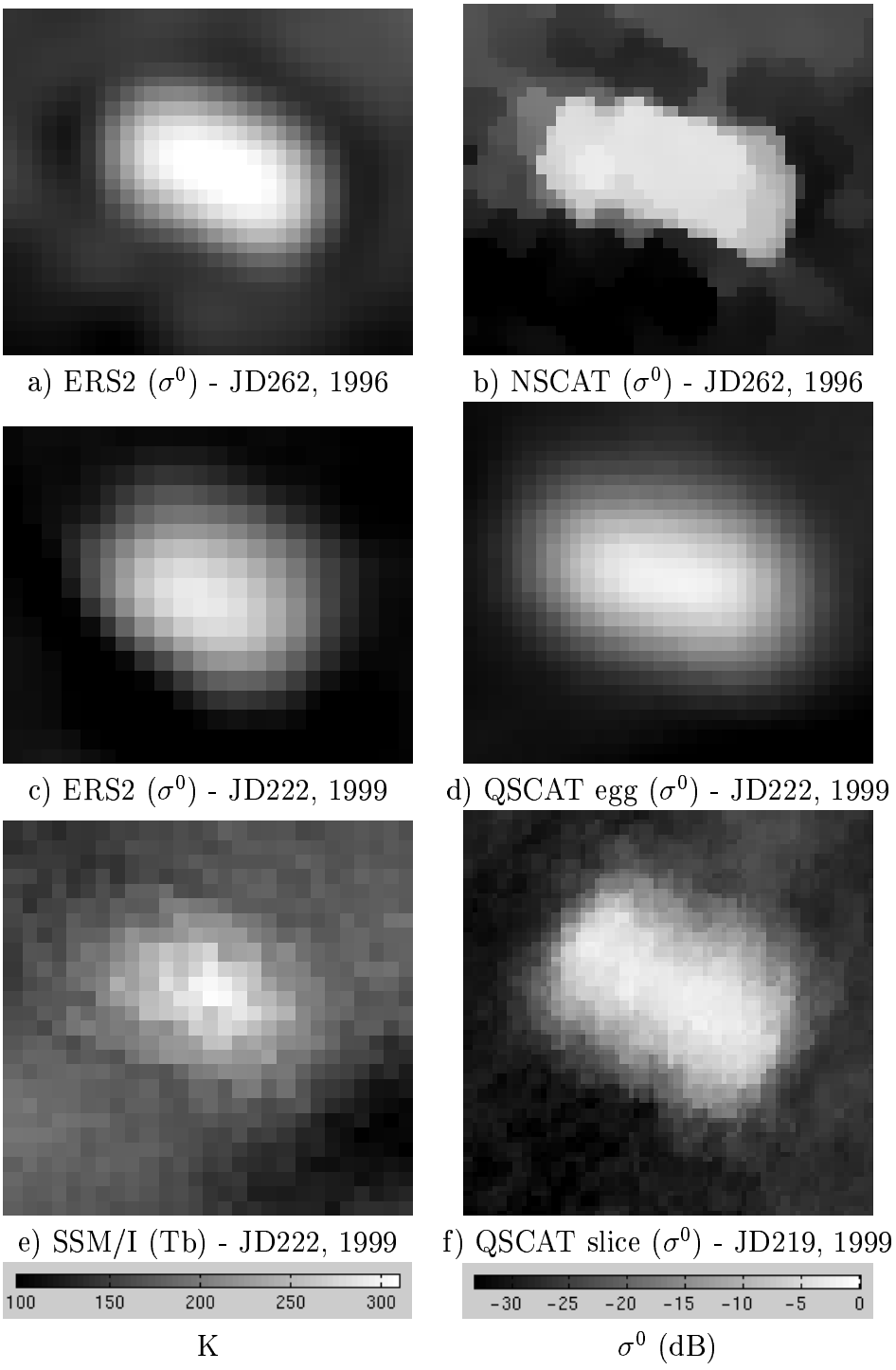

Figure 5.8: *Images of Iceberg B10A for different sensors.*

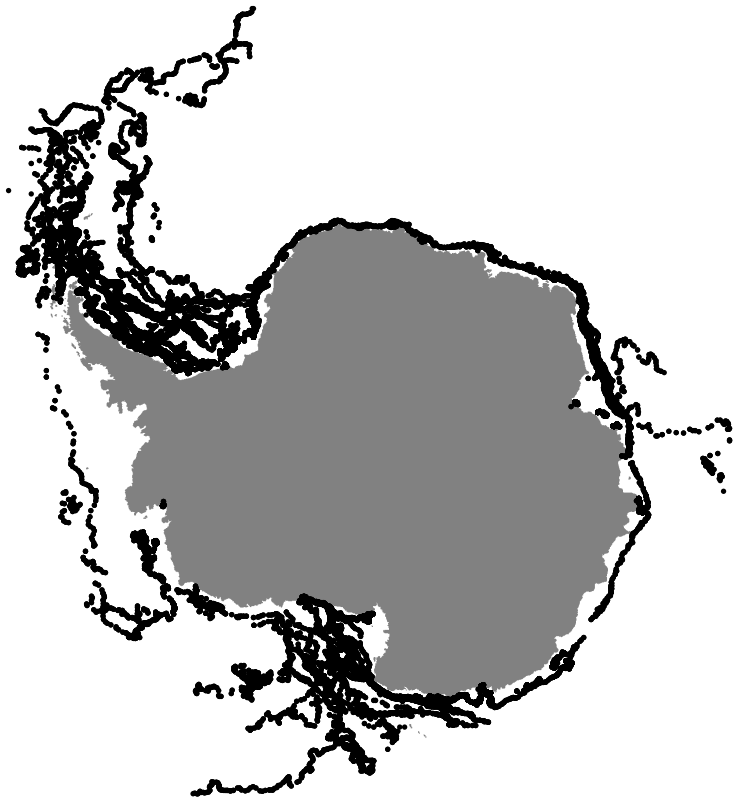

Figure 5.9: *All positions reported for all icebergs tracked by BYU (1978,1992-2001), shown as black dots.*

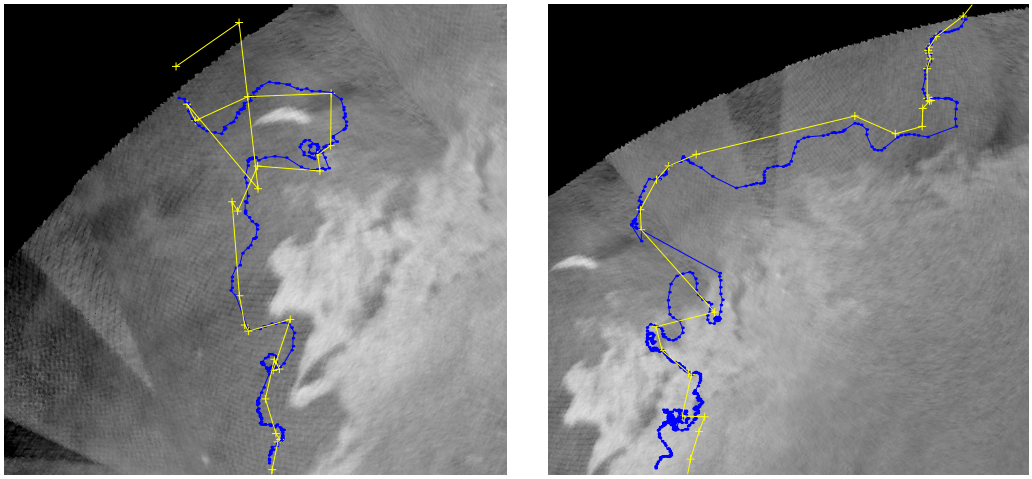

a) A22B b) A22C

Figure 5.10: *Tracks of two icebergs overlaying QSCAT images (BYU vs. the NIC).*

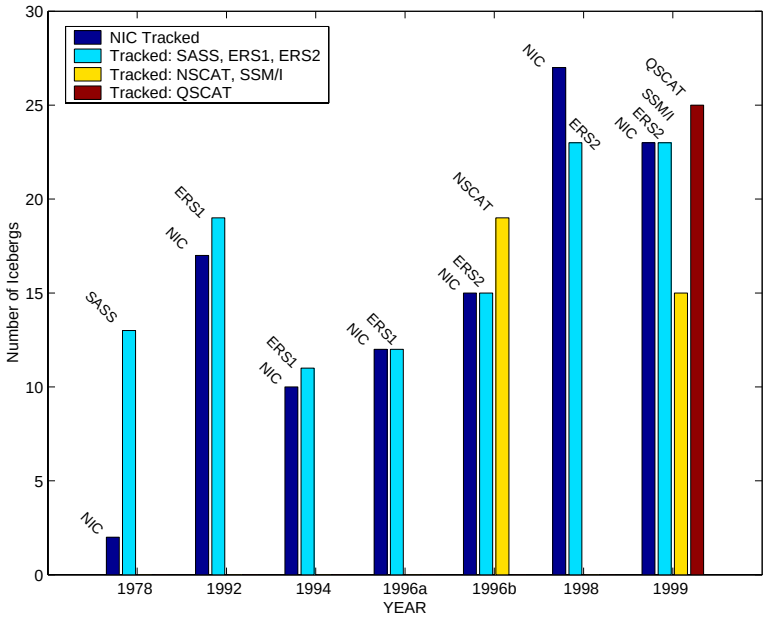

Figure 5.11: *Number of icebergs tracked at BYU vs. NIC.*

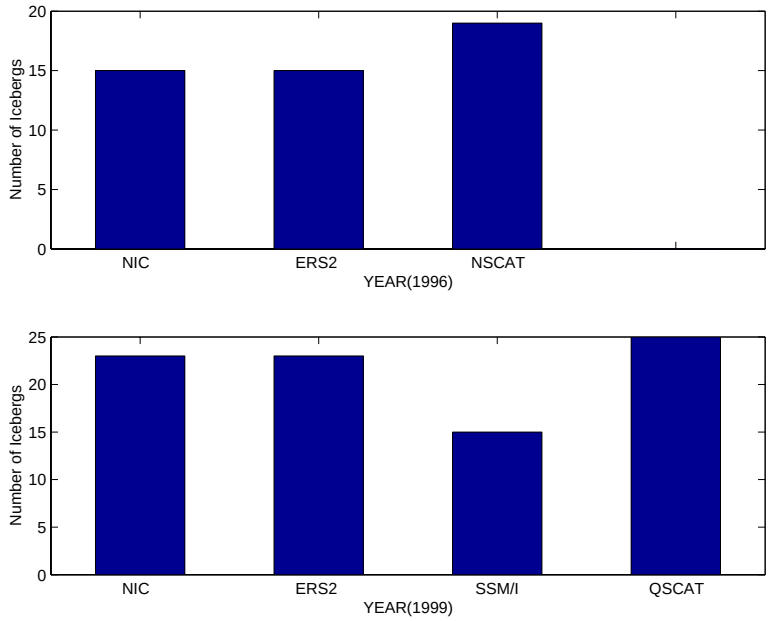

Figure 5.12: *A comparison of the number of icebergs tracked at NIC vs. icebergs tracked at BYU using various radar instruments during two different years.*

Chapter 6

Conclusion

This thesis has evaluated the utility of enhanced resolution scatterometer and radiometer images for the tracking and monitoring of large Antarctic icebergs. These images are evaluated for their usefulness in tracking icebergs and are compared with other iceberg tracking methods. A semi-automated tracking method has been developed and used to track many icebergs over a span of about 25 years. This extensive iceberg database is used to evaluate the change in the number of icebergs over the last two and a half decades.

6.1 Summary of Contributions

Several significant contributions have been made to the study of Antarctic icebergs using remote sensing. The following sections briefly summarize each of the major contributions of this thesis.

6.1.1 Using Passive Radiometer Data to Track Icebergs

In Chapter 3 seven SSM/I frequency channels are evaluated for tracking several Antarctic icebergs. Although higher frequency channels provide a better resolution than low frequency channels, they are noisier due to the high frequency sensitivity to atmospheric distortions. Lower frequency channels have coarser resolution but are not as noisy. Ability to track each iceberg is determined. The lower frequency (lower resolution) images are determined to be optimal for tracking Antarctic icebergs. However, higher frequency images are useful for tracking smaller icebergs.

Studying the differences in T_b distributions for each frequency channel revealed some interesting observations. These differences result from changes in sensitivity due to summer ice melt and to differences in emissivity for horizontally and vertically polarized images. Iceberg T_b values are generally lower than sea ice T_b values due to the physical characteristics of each type of ice.

6.1.2 Utilizing QuikSCAT Data to Track Antarctic Icebergs

In Chapter 4, enhanced resolution scatterometer images obtained from the SeaWinds on QuikSCAT scatterometer are evaluated for their usefulness in tracking and monitoring large Antarctic icebergs. With the help of the SIR algorithm, a set of enhanced resolution images are produced from SeaWinds σ^0 data. Icebergs are generally readily visible due to the contrast in σ^0 between icebergs and ocean or sea ice. The SIR algorithm produces both egg and slice SIR and AVE images for both h-pol and v-pol observations. Each image type has its advantages and limitations for tracking icebergs. The h-pol images are better than v-pol images due to the higher contrast σ^0 between icebergs and surrounding ocean. Egg-based SIR images perform better than egg-based AVE images because of the improved resolution of the SIR processing. Slice-based images perform better than all egg-based images due to the higher spatial resolution. Slice-based AVE images provide the best results because of higher resolution and lower noise characteristics.

Several observations are made by examining the distribution of σ^0 values for icebergs. The distribution of σ^0 values versus time for all icebergs is bimodal due to increased melt in summer months from higher temperatures. Understanding the melt pattern aids in visual recognition of icebergs during the Antarctic summers.

Antarctic katabatic winds have an important relationship with ice shelves and icebergs in creating bottom water which plays a crucial role in the earth's weather system. If the number of icebergs increases due to polar warming, katabatic winds may assist in the formation of sea ice around these icebergs creating more bottom water than normal. This may significantly affect the system of global ocean currents which impacts weather patterns and climate throughout the world. QSCAT images are a valuable tool for studying this phenomenon.

6.1.3 A Multidecadal Study of Antarctic Icebergs Using Scatterometer Data

Chapter 5 studies the number of Antarctic icebergs tracked over the last 25 years. The number of icebergs tracked by the NIC has risen over the last two decades. This increase is due to several recent iceberg calving events, to improved resources for iceberg tracking, and/or to technological advancements. To evaluate the NIC's results and monitor iceberg activity, BYU utilized scatterometer and radiometer data to track icebergs over the last 25 years. Icebergs were tracked independently with each data set. The result is an increasing trend in the number of visible icebergs. The increasing trend is visible after 1999-2001 due to several major calving events. However, from 1978-1998 the number of icebergs tracked remains fairly constant. Whether or not the recent increase represents a natural variability is unknown. More data is needed to determine if this is the case.

This study has also shown the advantages and limitations of tracking icebergs with methods used by the NIC versus methods used at BYU. Iceberg tracking at BYU has resulted in the discovery of many new icebergs over the years. It has extended the tracking capabilities for many existing icebergs.

6.2 Future Research

The motion of very large icebergs is influenced primarily by ocean currents [33]. Tracking the motion of icebergs will give an indication of mean current speed and direction. With the information currently obtained in BYU's extensive iceberg database a study of iceberg motion may reveal some new insights to Antarctic ocean currents. The knowledge of average Antarctic current speed and direction may be useful to understanding a larger system of global ocean currents which regulate much of the Earth's climate.

As shown by [34] the forces on large deep icebergs are dominated by ocean currents and the coriolis force. It has also been shown that a lift force can be exerted on an iceberg that is in steady translational motion. The lift force exerted by the sea is of the same order of magnitude as the coriolis force and can effect the velocity of

large icebergs. If the iceberg rotates anti-clockwise in the southern hemisphere the lift force is in the opposite direction as the coriolis force. Therefore the velocity of an iceberg is reduced. It has been observed that with the help of enhanced resolution scatterometer images and the iceberg database that the rotation of several Antarctic icebergs may be calculated. It is then possible to determine if the rotation of these icebergs has an effect on their velocity.

Appendix A

Antarctic Iceberg Tracking Database

While designed for remotely measuring winds over the ocean, data from the SeaWinds on QuikSCAT scatterometer is also useful in mapping sea ice extent, and tracking large icebergs. This appendix describes an extensive database of Antarctic iceberg positions starting with Julian Day (JD) 202, 1999 generated from SeaWinds data. It also describes algorithms implemented in Matlab used for tracking Antarctic icebergs using polar images generated by SeaWinds.

A.1 Background

SeaWinds measures the normalized radar backscatter cross-section (σ^0) of the Earth's surface at Ku-band (13.6 GHz). Two types of measurements are generated: "eggs", which have a nominal resolution of 25x30 km, and "slices", which have a nominal resolution of approximately 6x25 km. Eggs and Slices are collected on an irregular grid over a 1800 km wide swath. By combining multiple orbit passes, the Scatterometer Image Reconstruction (SIR) algorithm [26] or AVE algorithm [25] is used to make enhanced resolution images of the surface backscatter. The grid spacing for egg-based images is nominally 4.45 km while the slice-based images used for near real-time (NRT) process have a 2.225 km/pixel spacing. Images are produced in a polar stereographic projection with reference latitude of 70 degrees. The effective resolution of the images is somewhat less than this, depending on the number of orbit passes. NRT images of the radar cross-section are being used to operationally map the daily extent of sea-ice at the National Ice Center (NIC).

Glacial ice, from which most large icebergs are made, has a larger backscatter cross-section than sea-ice. This contrast difference makes it possible to identify icebergs in the sea-ice cover. Using daily polar images from SeaWinds, position updates for large icebergs can be generated which are nearly unaffected by weather conditions or time of day.

There are some ambiguities to viewing icebergs with SeaWinds images. First, some of the surface contrast is lost when summer temperatures climb high enough to melt the surface of the glacial ice and sea-ice. During such periods it may not be possible to accurately identify the iceberg center position within the sea ice or open ocean. Second, over the ocean the surface cross-section is a function of the near-surface wind velocity. Wind speed is monotonically related to σ^0. Low wind speeds result in small σ^0 values while high wind speeds produce a much higher backscatter cross-section. Since several orbits are combined when generating the enhanced resolution backscatter images and the wind can be highly variable, open ocean often appears as a mottled surface. Contrast between the wind-roughened ocean surface and iceberg depends on the wind conditions and the iceberg surface melt conditions. Generally, icebergs are visible, though position estimates can be very uncertain when high temperature and high wind speeds are encountered.

A.2 The Semi-Automated Tracking Program

A semi-automated technique for locating iceberg positions has been developed, which has been verified against subjectively located positions. For the MERS data set egg-based AVE images and Near Real Time (NRT) slice images were used to track most of the Southern Hemisphere icebergs named in the National Ice Center (NIC) database. The initial position for each iceberg is located based on either the position reported by NIC's web page (URL: http://www.natice.noaa.gov/) or by the first recorded sightings of new icebergs found at BYU. Each iceberg is then located within the SeaWinds image using the MERS program for tracking Icebergs (Appendix B). This procedure is followed for all icebergs. Gaps in the time series result from missing SeaWinds data and from loss of contrast between the iceberg and surrounding area. For each day a lat/lon position is reported.

Positions are reported in a separate ASCII text file for each iceberg. Each file name is the same as that of the iceberg. For example the file b10a.datc contains the position track information for B10A from JD202, 1999 until its breakup in early 2000. A few lines from the b10a file are shown below:

lat: -73.1882 lon: -35.028 x: 1460 y: 2608 file: qush-Ant-a-20010180044-20010182252.ave
lat: -73.2415 lon: -34.984 x: 1462 y: 2606 file: qush-Ant-a-20010190011-20010192339.ave
lat: -73.2415 lon: -34.984 x: 1462 y: 2606 file: qush-Ant-a-20010200125-20010202333.ave
lat: -73.2780 lon: -35.095 x: 1462 y: 2604 file: qush-Ant-a-20010210053 20010212301.ave

Note that latitude and longitude are specified in decimal degrees with positive North and East, respectively. The next two numbers are the x and y pixel coordinates of the image where the iceberg is located. The last section contains the name of the image that was used to track the selected position.

A.2.1 First Semi-automated Tracking Method

Due to the unpredictable nature of iceberg movement it was found that iceberg tracking algorithms are useful for locating the positions of large Antarctic icebergs. Two semi-automated tracking algorithms were developed and are described below.

The first semi-automated tracking algorithm was designed to locate icebergs in the enhanced resolution time series of scatterometer images [35]. A training sample image of the iceberg from the first image is located and entered as input to the algorithm. By using the initial sample image the iceberg is located in the next image by calculating the cross-correlations in the area of the previous image. The icebergs position is chosen as the point with the highest correlation and proximity. The training sample image for locating the iceberg in the next image in the sequence is selected as a window around the new iceberg's selected position. The widow size is calculated to be slightly bigger than the maximum distance that the iceberg was likely to travel between images. The requirements for choosing the iceberg location (t_1, s_1) in the $(i+1)th$ image is given by [35],

$$R_{X_i W_{i+1}}(t_1, s_1) = Max\{R_{X_i W_{i+1}}(t, s))\}$$

$(|t_1|, |s_1|) = Min\{|t|, |s|\}$

where

$R_{X_i W_{i+1}}(t, s)) = Correlation\ function\ between$
$the\ training\ sample\ and\ the\ image$

$X_i = training\ sample\ from\ ith\ image$

$W_{i+1} = window\ from\ (i+1)th\ image.$

This algorithm performs well for most of the year and is significantly improved when land features are masked out of the image. However during the Antarctic summer the iceberg merges with the generally low backscatter background due to surface melting. For icebergs such as B10A and A22B it was found that the locations selected with this algorithm were approximately 70-80% accurate. It was also found that due to iceberg rotation this algorithm's cross-correlation function could be improved by rotating the training sample image several degrees between cross-correlation calculations. The selected position is chosen as the point of highest correlation for all of the cross-correlation matrices produced. However this adaptation to the algorithm did little to improve the accuracy of the selected positions.

A.2.2 Second Semi-automated Tracking Method

Another similar semi-automated tracking algorithm developed to locate icebergs and was found to be more effective than the first method. An initial iceberg position is used as input to the algorithm. After land features are masked out of the image, a window centered around the icebergs position is then created in the next image. The size of the window is also selected to be slightly larger than the maximum distance that the iceberg will likely travel between images. The location of the iceberg is selected as the position where the σ^0 value is the highest. The requirements for choosing the (t_1, s_1) position in the $(i+1)th$ image is given by,

$\Omega_{i+1}(t_1, s_1) = Max\{\Omega_{i+1}(t, s)\}$

$(|t_1|, |s_1|) = Min\{|t|, |s|\}$

where

$\Omega_{i+1}(t, s)) = Window\ of\ \sigma^0\ values\ from\ the\ (i+1)th\ image.$

Because the σ^0 value for icebergs is almost always higher than sea water or sea ice this algorithm provides accurate results. For icebergs such as B10A and A22B it was found that the positions selected with this algorithm were about 80-90% accurate. However it was also found that this algorithm also fails during the Antarctic summer months. Due to the success of this algorithm it is currently being used in the semi-automated iceberg tracking program described below.

Appendix B

The Semi-Automated Tracking Program

A matlab program has been created tracking Antarctic icebergs using Sea-Winds images. This program must be in the same directory as the images used in tracking the icebergs. The Antarctic masked image file test3mask.lmsk is required to be in this same directory. This mask file provides information for the program's auto tracking capabilities. The iceberg files are also located in this directory. The iceberg files should have a .datc extension for the tracking program to recognize them. Files with the extension of .dat are old icebergs no longer tracked in the database. Add icebergs to this database or archive by selecting option two from the tracking program (See below). The iceberg file name must be four characters long with the .datc extension. (i.e. d015.datc, b09b.datc etc).

To start the program type the name of the matlab program file at the Matlab prompt. If successful a menu will appear as shown in Figure B.1. To select an option simply type the number for the correct option and hit Enter.

B.0.3 Option 1

This option will allow the user to update the position for each iceberg in the tracking database. The program will check the iceberg file for the last image used in tracking the icebergs position and compare it with all other images in the directory. If there are no new images the program will skip to the next iceberg in the database and a message will appear specifying the iceberg has an up-to-date position database (i.e. Iceberg a027.datc has an up-to-date database). If the program finds new images three matlab figures will appear.

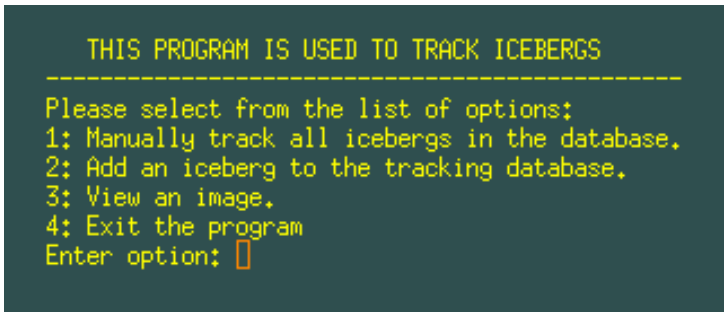

Figure B.1: *The Main Menu for the Iceberg Program.*

To illustrate, Figure B.2 contains a portion of the image were the iceberg should be located. The name of the iceberg, the year, and the day of the image are located at the top of the image. A blue circle indicates the last known position for the particular iceberg. A red X indicates the program's best guess as to where the iceberg is located. The red X may not always be accurate. It generally only works for icebergs that are located a finite distance from the Antarctic continent and for icebergs that are not located near any other icebergs. The green + is the current selected location. To change the current location move the mouse to the location were the iceberg is and left click with the mouse. The green + then appears at this new position. To continue the program middle click or right click with the mouse button. A middle mouse click exits to the next image or iceberg in the database without updating the iceberg's position. This feature is helpful if the iceberg is not visible and a location cannot be determined. A right mouse click exits the image and updates the iceberg file with the appropriate position information. Press the Esc button any time while tracking an iceberg and the program will skip to the next iceberg in the database. However, this option only works for new versions of the iceberg tracking program.

Figures B.3 and B.4 provide helpful information for tracking the icebergs. Figure B.3 shows a zoomed image of the current selected position. The blue circle, red X, and green + are identical to Figure B.2. Figure B.4 provides information about

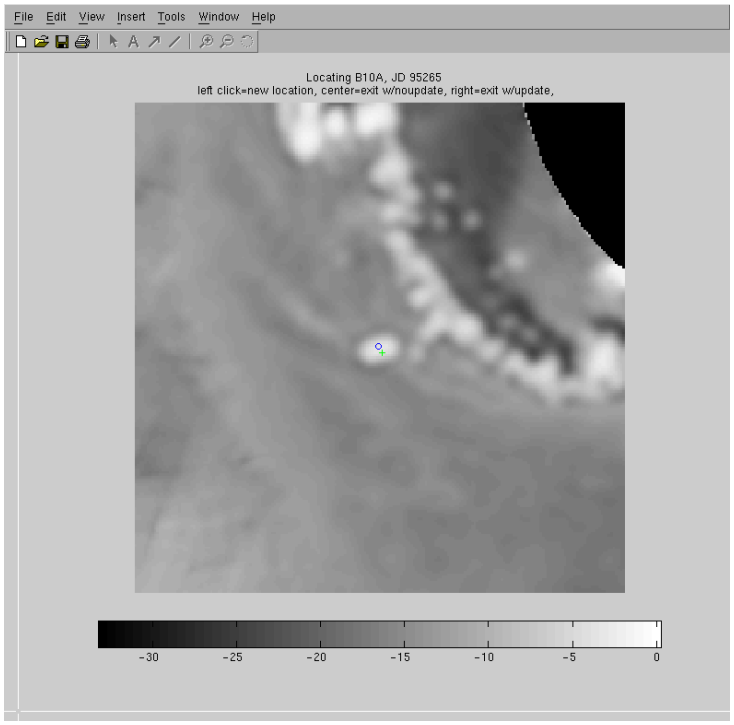

Figure B.2: *The Iceberg Tracking Program's Figure for Selecting Positions of Iceberg B10A (ERS image shown).*

the last recorded position for the iceberg, the current year and day of the image being used, the current position for the position selected with the green +, and the pixel value of the current position.

B.0.4 Option 2

This option allows the user to add an iceberg to the tracking database. This part of the program creates a file to contain the position information for the iceberg. The name of the file is the name of the iceberg (iceberg name must be at least 4 characters long) with a .datc extension. After selecting this option the program prompts the user to enter the name of the iceberg (i.e. b10a), the starting latitude and longitude coordinates, and the initial Julian Day and year (corresponding to the icebergs starting position). The latitude and longitude coordinates entered in should

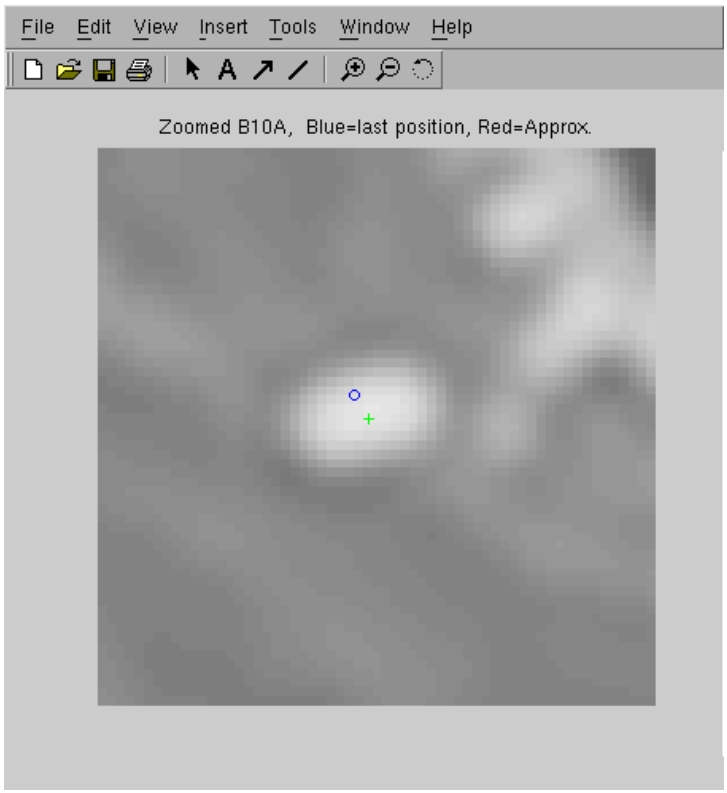

Figure B.3: *The Iceberg Tracking Program's Figure Showing the Zoomed Image of Iceberg B10A (ERS image shown).*

be in decimal format (i.e. -62.19). South latitude and West longitude should be entered in as negative values. If these values are not entered in correctly an error message appears and the program returns to the main menu. If each value is entered in correctly then the program creates a new file containing the icebergs initial position information.

B.0.5 Option 3 and 4

Option 3 allows the user to view an image in matlab. The program prompts the user to select the year and day to be viewed. If the image is not available the program selects the image closest to the day entered in. Because of its large size the image may take a few seconds to load. In the event the computer doesn't have

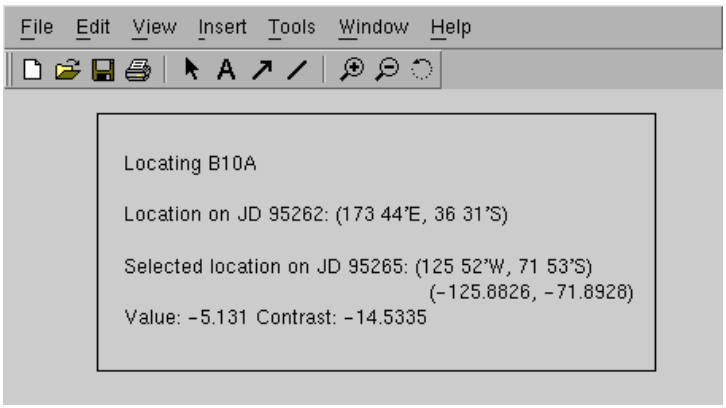

Figure B.4: *The Iceberg Tracking Program's Figure Displaying Key Information About the Iceberg.*

enough memory to load the image the program fails and exits with a memory error. Given the image loads successfully three figures appear. One figure displays the entire image for the selected day. A left mouse click selects a new location indicated by a green +. Another figure contains a zoomed-in image centered around the position selected. The Last figure contains information about the year, the day, the selected position in latitude and longitude, and the value of the pixel selected. A right click exits the image and returns to the main menu of the program. Option 4 simply exits the program and returns to the matlab prompt.

Bibliography

[1] R. Massom, *Satellite Remote Sensing of Polar Regions*. London: Belhaven Press, 1991.

[2] F. T. Ulaby, R. K. Moore, and A. K. Fung, *Microwave Remote Sensing*, vol. 1. Norwood, Massachesetts: Artech House, 1981.

[3] Q. P. Remund, "Multisensor microwave remote sensing in the cryosphere," tech. rep., Brigham Young University, 459 CB, Provo , UT 84602, 2000. PhD dissertation.

[4] P. J. Hardin, D. G. Long, Q. P. Remund, and D. R. Daum, "A comparison of reconstructed ku-band scatterometry, c-band scatterometry, and SSM/I imagery for tropical vegetation classification," tech. rep., Brigham Young University, 1999.

[5] D. Long and M. Dringkwater, "Greenland ice-sheet surface properties observed," *Journal of Glaciology*, vol. 40, no. 135, pp. 213–230, 1994.

[6] M. R. Drinkwater and D. G. Long, "Seasat, ERS-1/2 and NSCAT scatterometer observed changes on the large ice sheets," in *Proc. IGARSS*, vol. 4, (Seattle, Washington), pp. 2252–2254, July 6-10 1998.

[7] E. Attema, "The ative microwave instrument onboard the ERS-1 satellite," in *Proceedings of the IEEE*, vol. 79, pp. 791–799, 1991.

[8] F. Gohin and A. Cavanie, "A first try at identification of sea ice using the three beam scatterometer of ERS-1," *International Journal of Remote Sensing*, vol. 15, no. 6, pp. 1221–1228, 1994.

[9] F. Gohin, "Some active and passive microwave signatures of Antarctic sea ice from mid-winter to spring 1991," *International Journal of Remote Sensing*, vol. 16, no. 11, pp. 2031–2054, 1995.

[10] M. Drinkwater, D. Long, and D. Early, "Enhanced resolution ERS-1 scatterometer imaging of southern ocean sea ice," *ESA Journal*, vol. 17, pp. 307–322, 1993.

[11] D. S. Early and D. G. Long, "Azimuthal modulation of c-band scatterometer σ^0 over southern ocean sea ice," *IEEE Transactions on Geoscience and Remote Sensing*, vol. 35, no. 5, pp. 1201–1209, 1997.

[12] L. Ulander, A. Carlstrom, and J. Askne, "Effect of frost flowers, rough saline snow and slush on the ERS-1 SAR backscatter signatures of thin Arctic sea ice," *Int. J. Remote Sens.*, vol. 16, no. 17, pp. 3287–3305, 1995.

[13] D. G. Long and M. R. Drinkwater, "Cryosphere applications of NSCAT data," *IEEE Transactions on Geoscience and Remote Sensing*, vol. 37, no. 3, pp. 1671–1684, 1999.

[14] S. H. Yueh, R. Kwok, S. Lou, and W. Tsai, "Sea ice identification using dual polarised ku-band scatterometer data," *IEEE Transactions on Geoscience and Remote Sensing*, vol. 35, no. 3, pp. 560–569, 1997.

[15] M. R. Drinkwater and X. Liu, "Observing interannual variablility in sea-ice dynamics using nscat," in *Proceedings of NSCAT Science Team Workshop, Honolulu, Hawaii*, (4800 Oak Grove Drive, Pasadena, CA 91109), pp. 791–799, Jet Propulsion Laboratory, JPL Tech. Pub., 23-24 Jan. 1997.

[16] M. R. Drinkwater and D. G. Long, "Seawinds imaging of polar ice sheets," tech. rep., Jet Propulsion Laboratory, California Institute of Technology, Brigham Young University, 459 CB, Provo, UT 84602, 2000.

[17] M. W. Spencer, C. Wu, and D. G. Long, "Tradeoffs in the design of a spaceborne scanning pencil beam scatterometer: Application of seawinds," *IEEE Transactions on Geoscience and Remote Sensing*, vol. 35, January 1997.

[18] H. Zwaly, J. Cosmiso, C. Parkinson, W. Campbell, F. Carsey, and P. Gloersen, "Antarctic sea ice, 1973-1976: satellite passive-microwave observations," Tech. Rep. NASA Report SP-459, NASA, 1983.

[19] W. L. Grantham, E. M. Bracalente, W. L. Jones, and J. W. Johnson, "Seasat-A satellite scatterometer," *IEEE Journal of Oceanic Engineering*, vol. OE-2, April 1977.

[20] M. R. Drinkwater and F. D. Carsey, "Observations of the late-summer to fall transition with the 14.6 GHz SEASAT scatterometer," in *Proc. IGARSS '91 Symposium*, vol. 3, (Espoo, Finland), pp. 1597–1600, June 3-6 1991.

[21] J. Hollinger, "DMSP special sensor microwave/imager calibration/validation final report, volume 1," tech. rep., Naval Research Laboratory, Washington, D.C., July 1989.

[22] D. J. Cavalieri, J. P. Crawford, M. R. Drinkwater, D. T. Eppler, L. D. Farmer, R. R. Jentz, and E. C. Wackerman, "Aircraft active and passive microwave validation of sea ice concentration from the Defence Meteorological Satellite Program Special Sensor Microwave Imager," *Journal of Geophysical Research*, vol. 96, no. C12, pp. 21989–22008, 1991.

[23] D. G. Long and D. L. Daum, "Spatial resolution enhancement of SSM/I data," *IEEE Transactions on Geoscience and Remote Sensing*, vol. 36, pp. 407–417, March 1998.

[24] M. R. Farrar and E. A. Smith, "Spatial resolution enhancement of terrestrial features using deconvolved SSM/I brightness temperatures," *IEEE Transactions on Geoscience and Remote Sensing*, vol. 30, pp. 349–355, March 1992.

[25] D. Long, P. Hardin, and P. Whiting, "Resolution enhancement of spaceborne scatterometer data," *IEEE Transactions on Geoscience and Remote Sensing*, vol. 31, pp. 700–715, 1993.

[26] D. G. Long, "Standard BYU Quikscat/Seawinds land/ice image products," tech. rep., Brigham Young University, 459 Clyde Building, Provo, UT 84602, September 1999.

[27] D. S. Early and D. G. Long, "Image reconstruction and enhanced resolution imaging from irregular samples," *IEEE Transactions on Geoscience and Remote Sensing*, vol. 39, pp. 291–302, Febuary 2001.

[28] http://www.usatoday.com/weather/antarc/sun/2001-01-30-katabatic winds.htm, "Antarctic winds vital to global sea life," 2001.

[29] http://www.auburn.edu/∼coopegp/pol.html, "Polar air circulation," 2000.

[30] http://www.antarctica.org/UK/Envirn/pag/vents_cata_UK.htm.

[31] http://nsidc.org/iceshelves/, "Antarctic ice shelf collapse is triggered by warmer summers, melt water," 2001.

[32] http://www.colorado.edu/PublicRelations/NewsReleases/2001/1008.html, "Antarctic ice shelf collapse triggered by warmer summers," 2001.

[33] N. W. Young, "Antarctic iceberg drift and ocean currents derived from scatterometer image series," in *Proc. of a Joint ESA-Eumetsat Workship on Emergin Scatterometer Applications*, pp. 125–132, November 1998. ESA SP-424.

[34] M. Crepon and M. N. Houssais, "The drift of icebergs under wind action," *Journal of Geophysical Research*, vol. 93, pp. 3608–3612, April 1988.

[35] H. Stephen and D. G. Long, "Study of iceberg B10A using scatterometer data," *IEEE Transactions on Geoscience and Remote Sensing*, vol. 3, pp. 1340–1342, 2000.

[36] D. G. Long, M. R. Drinkwater, B. Holt, S. Saatchi, and C. Bertoia, "Global ice and land climate studies using scatterometer image data," *EOS, Transactions, American Geophysical Union*, vol. 82, no. 43, p. 503, 2001.